DNA breaks-mediated cost reveals RNase HI as a new target for selectively eliminating antibiotic resistance

Roberto Balbontín*[1], Nelson Frazão[1] and Isabel Gordo*[1]

[1] Instituto Gulbenkian de Ciência; Oeiras, 2780-156; Portugal

* Correspondence: rbalbontin@igc.gulbenkian.pt, igordo@igc.gulbenkian.pt

Abstract

Antibiotic resistance often generates a fitness cost to bacteria in drug-free environments. Understanding the causes of the cost is considered the Holy Grail in the antibiotic resistance field, as it is the main determinant of the prevalence of resistances upon reducing antibiotics use. We show that DNA breaks can explain most of the variation in the cost of resistances common in pathogens. Here we demonstrate that targeting the RNase that degrades R-loops, which cause DNA breaks, exacerbates the cost of resistance. Consequently, lack of RNase HI function drives resistant clones to extinction in populations with high initial frequency of resistance, both in laboratory conditions and in a mouse model of gut colonization. Thus, RNase HI provides a target specific against resistant bacteria, which we validate using a repurposed drug. In summary, we revealed key mechanisms underlying the cost of antibiotic resistance that can be exploited to specifically eliminate resistant bacteria.

Keywords

antibiotic resistance; fitness cost; DNA breaks; RNase HI targeting; repurposed drug.

Introduction

Antibiotic resistance entails a large health and economic burden worldwide (1). Its maintenance and spread in bacterial populations depend on the rate at which resistance is acquired and on its effect on bacterial fitness. This effect is typically deleterious, resulting in the so-called cost of resistance. The cost of resistance is influenced by the environment, by interactions between the resistances and the genetic background in which they appear (epistasis), and by subsequent acquisition of mutations compensating for fitness defects (compensatory evolution) (2). Importantly, the magnitude of the cost is the main biological parameter influencing the fate of resistances upon reducing antibiotic use (3). Despite its importance, the causes of the cost are far from being completely understood (4), and the identification of these causes has become the "Holy Grail" in the antibiotic resistance field.

Resistance mutations often map to genes encoding proteins targeted by antibiotics. These target proteins are typically involved in essential functions, such as transcription, translation, DNA replication or cell wall biosynthesis. Resistance mutations cause alterations in the structure of the target protein, rendering it insensitive to the drug, but often adversely affecting its function (2,3,5). These pleiotropic effects hold the key to manipulating resistance levels in bacterial populations (3). Rifampicin and streptomycin resistance mutations (Rif^R and Str^R), common in pathogenic bacteria (6–8), map to the genes *rpoB* and *rpsL*, encoding the β' subunit of the RNA polymerase and the protein S12 of the 30S ribosomal subunit, respectively. Rif^R and Str^R mutations are representative examples of resistances to antibiotics targeting transcription and translation, respectively. Rif^R mutations show different costs (9,10) and cause alterations in the rates of transcription initiation, elongation, slippage or termination (9,11–23). Likewise, most Str^R mutations also cause a cost (24–26) and affect translation fidelity and processivity (24,26–34). Thus, at present, the costs of Rif^R and Str^R mutations are thought to be caused

by defects in protein synthesis, either at a global cellular level (35–37) or limited to specific functions or regulons (22,24,38,39).

We recently showed that the fitness cost of double resistance (Rif^R Str^R) can be reduced via overexpression of *nusG* or *nusE (40)*, which encode the proteins that physically connect the RNA polymerase and the ribosome (41). This suggests that the reduction of the cost can be achieved by reinforcing the coupling between transcription and translation, besides the previously described partial recovery in protein biosynthesis (3). Coupling between transcription and translation is known to prevent spontaneous backtracking of the RNA polymerase which, if exacerbated, can cause a series of molecular events that ultimately lead to the generation of double-strand DNA breaks (42–46). This led us to hypothesize that cells carrying different Rif^R and Str^R mutations have higher number of DNA breaks, which greatly contribute to their cost.

In this study, we show that DNA breaks caused by resistance mutations are major contributors to their fitness cost, explaining 73% of its variation across resistant genotypes. The involvement of R-loops in the generation of DNA breaks allowed us to identify RNase HI as an important determinant of the cost of resistance, which we validate using a repurposed drug. We further show that targeting RNase HI is a plausible strategy for the selective elimination of resistant bacteria, as lack of RNase HI leads to extinction of resistant clones when competing against sensitive bacteria in laboratory conditions, abolishing compensatory evolution. Importantly, eradication of resistant bacteria lacking RNase HI is remarkably efficient in the mammalian gut as well. Altogether, we reveal an unexpected cause of the cost of antibiotic resistance, which can be exploited to selectively eliminate resistant bacteria in polymorphic populations.

Results

99

100 DNA breaks explain variation in the fitness cost of resistance

101

102 In order to test if Rif^{R} and Str^{R} mutations generate DNA breaks, and whether DNA breaks
103 contribute to the cost of resistance, we simultaneously measured competitive fitness and activation of
104 the SOS response, a well-known proxy specific for the occurrence of DNA breaks (47,48). We carried
105 out these assays in sensitive *Escherichia coli*, Str^{R} strains (RpsL^{K43N}, RpsL^{K43T}, and RpsL^{K43R}), Rif^{R}
106 strains (RpoB^{H526L}, RpoB^{H526Y}, and RpoB^{S531F}), and double resistant mutants carrying the nine possible
107 combinations of these resistance alleles. Remarkably, fourteen out of the fifteen resistant strains show
108 increased SOS activation (Figure 1A), demonstrating that resistance mutations indeed cause DNA
109 breaks. Moreover, the SOS induction strongly correlates with the cost of resistance, explaining 73% of
110 its variation (Figure 1B), suggesting that DNA breaks are key contributors to the cost of resistance. To
111 independently confirm the occurrence of DNA breaks in resistant bacteria, we used a system which
112 permits direct visualization of double-stranded DNA ends by fluorescence microscopy (49). We
113 combined this system with the SOS reporter, and analyzed a subset of resistant mutants and sensitive
114 bacteria. As expected, this corroborated that resistance mutations indeed cause increased number of
115 DNA breaks (Table 1, Figure S1). We then asked if resistance mutations involving a different
116 mechanism which could lead to perturbations of transcription-translation coupling also generate DNA
117 breaks. The commonly used antibiotic erythromycin targets the 50S ribosomal subunit, affecting
118 translation and its coupling with transcription (50). Erythromycin resistance mutations (Erm^{R}) mapping
119 to the genes *rplD* and *rplV* (encoding the 50S ribosomal subunit proteins L4 and L22, respectively) are
120 known to reduce translation elongation rate (51,52), likely affecting transcription-translation coupling.
121 We isolated Erm^{R} clones carrying either RplD^{G66R} or RplV$^{\Delta(82\text{-}84)}$ mutations and found that both mutants
122 show fitness cost and increased SOS (Figure 1C), demonstrating that other resistance mutations, with a

different mechanistic basis but affecting the same process (transcription-translation coupling) also cause DNA breaks.

Compensatory evolution cause reduction of DNA breaks

We then hypothesized that, if DNA breaks are key contributors to the fitness cost of resistance, compensatory evolution of resistant strains should result in a reduction of DNA breaks. To test this, we compared the cost and SOS induction in the RpsL^{K43T} RpoB^{H526Y} double mutant and in an isogenic strain additionally carrying the most prevalent compensatory mutation found in our previous study: RpoC^{Q1126K} (40). As hypothesized, both cost and SOS induction are greatly reduced in the compensated strain (Figure 2A), confirming that DNA breaks are targeted by compensatory evolution. In order to test if this is general, we analyzed nine compensated clones from three independent populations of the RpsL^{K43T} RpoB^{H526Y} double mutant propagated for fifteen days in the absence of antibiotics. As expected, the costs are smaller in the evolved strains and, as hypothesized, all the nine compensated clones show decreased SOS induction compared to their resistant ancestor (Figure 2B). This demonstrates that compensatory evolution widely targets mechanisms that reduce DNA breaks and further reinforces the notion that DNA breaks are major contributors to the cost of antibiotic resistance.

Increasing transcription-coupled DNA repair reduces the cost of resistance

We then hypothesized that, if DNA breaks contribute to the cost of resistance, enhancing DNA repair should reduce the cost. The RNA polymerase-binding transcription factor DksA has been recently shown to be involved in the transcription-coupled repair of DNA breaks (53,54). Thus, we hypothesize that overexpression of *dksA* should decrease the cost of resistance. As hypothesized, overproduction of DksA increases the fitness of the double resistant RpsL^{K43N} RpoB^{H526Y}, but not that of

148 sensitive bacteria (Figure S2A), indicating that the relationship between DNA breaks and the fitness
149 cost of antibiotic resistance is, indeed, causal.
150
151 Replication speed affects the cost of resistance
152
153 Transcription-translation uncoupling can involve increased generation of replication-
154 transcription conflicts, which ultimately generate DNA breaks (42,55). Replication-transcription
155 conflicts are maximized during fast replication, and less pronounced when bacteria grow slowly (56).
156 Consequently, we hypothesized that the cost of resistance should be expressed mostly when cells are
157 rapidly dividing. Indeed, we observed that, although the costs of Rif^R and Str^R mutations are similar at
158 4h and 24h, these costs are generated in the first 4 hours (which comprise exponential growth), while
159 resistance mutations show no cost afterwards, when growth slows down (Figure 3A). We therefore
160 hypothesize that altering replication-transcription conflicts should affect the fitness cost of resistance.
161 To test that hypothesis, we influenced the occurrence of replication-transcription conflitcs through two
162 strategies: negatively by growing our set of mutants in minimal medium, where DNA replication is
163 slower (57), or positively it by overexpressing the DNA replication initiator protein DnaA, which
164 causes simultaneous initiation of multiple replication forks (58). Our hypothesis predicts that DNA
165 breaks should be reduced in minimal medium, where replication-transcription conflicts are less
166 pronounced (Figure 3B). In agreement with our hypothesis, the SOS induction is smaller in minimal
167 than in rich media (Figure 3C, right panel), and the correlation with the cost is much weaker in minimal
168 medium (Figure S2B). Coherently, the number of resistant mutants showing a fitness cost is smaller in
169 minimal medium (8, compared to 13 in rich medium), with four of them even showing a higher fitness
170 than sensitive bacteria (Figure 3C, left panel). Moreover, some of the most costly mutations in rich
171 medium (e. g. $RpsL^{K43N}$ $RpoB^{H526Y}$ and $RpsL^{K43T}$ $RpoB^{H526Y}$) generate a much smaller cost in minimal
172 medium (compare Figure 1A with Figure 3C). Besides this general trend, however, there are resistant

173 mutants (notably, those carrying the allele RpoB^{S531F}) that conserve or even increase their fitness cost in
174 minimal medium (compare Figure 1A with Figure 3C), evidencing the existence of additional factors
175 contributing to the cost of resistance (such as the known defects in protein synthesis). Conversely, our
176 hypothesis also anticipates that increasing the occurrence of replication-transcription conflicts by
177 overexpressing DnaA should particularly affect resistant bacteria. As hypothesized, overexpression of
178 *dnaA* severely compromises the viability of double resistant bacteria, whereas sensitive bacteria
179 remains largely unaffected (Figure 3D). Altogether, these results demonstrate the involvement of
180 replication-transcription conflicts in the generation of the cost of antibiotic resistance, also
181 corroborating the key contribution of DNA breaks to it.
182
183 RNAse HI strongly influences the fitness of resistant bacteria
184
185 Both transcription-translation uncoupling and replication-transcription conflicts lead to
186 increased formation of R-loops, which cause DNA breaks (42,59) and exacerbate replication-
187 transcription conflicts themselves by impairing replication fork progression (60). We thus reasoned that
188 depleting RNase HI function, which specifically degrades R-loops (61), should lead to increased DNA
189 breaks and greater costs of Rif^{R} and Str^{R}. Accordingly, both DNA breaks and the cost of resistance are
190 greatly exacerbated in the *ΔrnhA* background (Figure 4A, Table 1, Figure S3, Figure S4A). Conversely,
191 mild overproduction of RNase HI can ameliorate both phenotypes in a subset of mutants (Figure S5);
192 however, strong overproduction is toxic for the cell (62,63), irrespective of its genotype (Figure S6).
193 These results confirm the involvement of R-loops in the uncoupling-mediated production of DNA
194 breaks caused by resistance and suggest that RNase HI can be a target for manipulating the fitness of
195 resistant strains in bacterial populations.
196
197 RNase HI can serve as a target specific against resistant bacteria

198

199 The large effect of lacking RNAse HI function on the fitness of resistant bacteria prompted us
200 to ask whether targeting it could be used to select specifically against resistant bacteria in polymorphic
201 populations. RNase HI inhibitors are currently studied as antiretrovirals (64). A commercially available
202 one, RHI001, has been shown to inhibit the activity of purified *E. coli* RNase HI protein *in vitro (65)*.
203 In competitions between sensitive and resistant bacteria, we observed that addition of RHI001 to the
204 medium increases the cost of most resistant mutants (Figure 4B), on average by 14%. RHI001 also
205 reduces fitness of double resistant bacteria more than that of sensitive bacteria in the absence of
206 competition (Figure S4B and S4C). Chemical inhibition was not as effective as genetic removal (which
207 increases cost on average by 28%) (Figure 4C and D), as may be expected, since stability, diffusibility
208 across the bacterial envelope, pharmacokinetics and pharmacodynamics of RHI001 *in vivo* are
209 unknown, and potentially suboptimal. Nevertheless, these results suggest that inhibiting RNase HI may
210 be a plausible strategy to select specifically against resistant strains coexisting with sensitive bacteria,
211 as long as resistant strains fail to evolve adaptations that abrogate their extinction. In order to test this
212 hypothesis, we propagated a mixture of sensitive bacteria (CFP-labeled) competing against a pool of
213 five single resistant mutants (YFP-labeled $RpsL^{K43N}$, $RpsL^{K43T}$, $RpoB^{H526L}$, $RpoB^{H526Y}$, and $RpoB^{S531F}$)
214 during 15 days, in the absence of antibiotics. We studied the frequency dynamics of resistant clones
215 under both strong bottlenecks (1:1500 dilutions), where new adaptive mutations are less likely to
216 spread, and weak bottlenecks (1:50 dilutions), where propagation of adapted clones is more probable.
217 In parallel, we performed identical propagations, but in which all strains lack RNase HI, as a proxy for
218 optimal inhibition of RNase HI function. We observed that, in the presence of RNase HI, sensitive
219 bacteria initially outcompete resistant clones but, as the propagation progresses, resistant bacteria
220 increase in frequency - likely due to compensatory evolution - finally reaching coexistence (Figure 5A,
221 blue lines). Remarkably, in the propagations of strains lacking RNase HI, resistant bacteria were
222 completely outcompeted and went extinct by day seven (Figure 5A, red lines) even under mild

223 bottlenecks (Figure 5B). Since the outcome of competitions under laboratory conditions can differ from
224 those within the host (4,66), we next tested if inhibition of RNase HI would be an effective strategy in
225 an animal model. We used the well-established mouse gut colonization model, which resembles the
226 natural environment of many bacterial pathogens, including *E. coli* (67). We colonized by oral gavage
227 two cohorts of mice (each n=6): one with a 1:9 ratio mixture of CFP-tagged sensitive bacteria and a
228 YFP-labeled double resistant strain [$RpsL^{K43T}$ $RpoB^{H526Y}$, selected based on its ability to efficiently
229 colonize the mammalian gut (68)], and the other with an identical mixture but in which both strains are
230 *ΔrnhA*. We then followed the frequency and absolute numbers [Colony Forming Units (CFUs) per
231 gram of feces] of the resistant strain over time. Remarkably, when RNase HI function is intact, the
232 double resistant strain persists in the gut of all animals at frequencies between 2.3 and 9.3% (Figure 5C,
233 blue lines) and high bacterial loads (Figure 5D, blue lines) two weeks after gavage but, in the absence
234 of RNase HI, resistant clones are rapidly outcompeted by sensitive bacteria (Figure 5C and D, red
235 lines). Indeed, resistant bacteria are driven to extremely low frequencies in as soon as 1 day post-
236 colonization, and their extinction occurs in all the six mice in as soon as 5 days (Figure 5C and D, red
237 lines), demonstrating that RNase HI is a new target for efficiently eliminating resistant strains in the
238 gut. Surprisingly, the absence of RNase HI does not lead to any detectable fitness defect in the sensitive
239 bacteria, as the loads of *E. coli* are similar in the two cohorts of mice (Figure 5E). We then queried if
240 the sequential application of an RNase HI inhibitor followed by an antibiotic could successfully
241 eliminate the entire population of a potential gut pathogenic species composed of sensitive and resistant
242 strains. In this scenario, we hypothesize that an antibiotic treatment should render completely different
243 outcomes depending on the presence of RNase HI function. Indeed, a week-long treatment of
244 streptomycin starting at day 16 after gavage enables resistant clones with intact RNase HI function to
245 rebound and reach high loads (10^7-10^8 CFUs/g feces), but it completely erradicates *ΔrnhA* bacteria in
246 all the six mice (Figure 5F). These results demonstrate that RNAse HI function is not only a key
247 determinant of the fitness of resistant bacteria, but also a potential co-adjuvant to eliminate undesirable

248 bacteria in a natural environment for bacterial pathogens such as the mammalian gut. Altogether, these
249 results show the enormous potential of targeting RNase HI as a promising antimicrobial therapy.
250
251 **Discussion**
252
253 We show that mutations affecting transcription and translation generate DNA breaks, which
254 explain 73% of the variation in their cost (Figure 1, Table 1, Figure S1). Compensatory evolution
255 indicates that these resistances cause uncoupling between transcription and translation (40), which can
256 result in DNA breaks (42). Indeed, we show that the $RpsL^{K43N}$ $RpoB^{H526Y}$ and $RpsL^{K43T}$ $RpoB^{H526Y}$ double
257 mutants, which combine alleles that cause increased transcription elongation rate (12) and decreased
258 translation rate (26,69), show the highest costs and DNA breaks (Figure 1). Curiously, inhibition of
259 translation has been shown to alleviate the cost of Rif^R mutations in *Pseudomonas aeruginosa* (36). In
260 light of the results presented here, this observation is compatible with a scenario in which Rif^R
261 mutations cause a perturbation of transcription-translation coupling by virtue of reduced RNA
262 polymerase processivity, and translation inhibitors promote re-coupling by decreasing ribosomal
263 activity. In agreement with the notion of single resistance mutations causing significant uncoupling,
264 single Rif^R or Str^R mutations with high cost (70) cause a strong induction of the SOS response (Figure
265 S7). We also showed that RNase HI is a key determinant of the fitness of resistant mutants (Figure 4,
266 Table 1, Figure S3, Figure S4A, Figure S5, Figure S6). Interestingly, transcription-translation
267 uncoupling caused by chemical inhibition of translation can generate R-loops (42,71,72). Thus,
268 perturbations of the coupling between transcription and translation increase the requirement of RNase
269 HI function by bacteria. This opens the possibility to designing novel therapeutic interventions by
270 combining drugs targeting transcription or translation with RNase HI inhibitors in order to enhance the
271 effectiveness of antimicrobial treatments.
272

273 We observed that replication-transcription conflicts contribute to the cost of resistance (Figure
274 3), and that overproduction of DksA, involved in transcription-coupled DNA repair (53,54), reduces
275 the cost of resistance (Figure S2A). Interestingly, DksA is also involved in preventing replication-
276 transcription conflicts (73). Thus, prevention of the conflicts by DksA might also account for its
277 beneficial effect on resistant bacteria, besides the enhancement of DNA repair. The involvement of
278 replication-transcription conflicts in the cost of resistance is coherent with previous observations, such
279 as the small cost of specific Rif^R and/or Str^R alleles in minimal medium (24,74,75) or the
280 outcompetition of sensitive bacteria by resistant mutants in aging colonies (76,77). Interestingly, stable
281 DNA replication (initiation of DNA replication at sites different from *OriC*) can be induced by lack of
282 RNase HI or by conditions that activate SOS (78). Thus, Rif^R and Str^R mutations, which induce SOS
283 (Figure 1), could additionally favor replication-transcription conflicts via induction of stable DNA
284 replication. This can generate a feed-forward loop of synergistic deleterious effects, which may be
285 further enhanced by the fact that induction of the SOS response causes downregulation of *rnhA* (79).
286 This detrimental runaway loop, as well as the effects of the environment on the cost described above
287 (Figure 1A and Figure 3C), could potentially be exploited therapeutically, via concurrent chemical and
288 dietary treatments designed to synergistically maximize the cost of resistance.
289
290 We revealed RNase HI as a promising target specific against resistant bacteria (Figure 4), and
291 showed that lack of RNase HI function favors extinction of resistant clones, preventing compensatory
292 evolution (Figure 5A and B). Importantly, we demonstrated that targeting RNase HI leads to the
293 efficient elimination of resistant bacteria in an animal model as well (Figure 5C and 5D). Interestingly,
294 sensitive bacteria lacking RNase HI do not show fitness defects in the gut (Figure 5E), which hampers
295 the development of resistance to RNase HI inhibition. Moreover, targeting RNase HI prevents
296 recurrence of resistant bacteria upon an antibiotic treatment, favoring the elimination of the entire
297 bacterial population (Figure 5F). These notions are specially important for resistances mediated by

298 mutations (80) or for pathogens that acquire antibiotic resistance exclusively through mutation, such as
299 *Mycobacterium tuberculosis*, which often carries Rif^R and Str^R mutations (81). Interestingly, RNase HI
300 has been proposed as an antimycobacterial target due to its essentiality in *Mycobacterium smegmatis*
301 (82,83). The results presented here strongly support the plausibility of this strategy.
302
303 An understanding of the determinants of maintenance and dissemination of antibiotic resistance,
304 such as its cost, is urgently needed (1). We show that DNA breaks are key contributors to the cost of
305 resistance and reveal RNase HI as a promising antimicrobial target specific against resistant bacteria,
306 which we validated under laboratory conditions, in the mammalian gut, and by using a repurposed
307 drug. Overall, our results uncover important effects of resistances on bacterial physiology and
308 demonstrate the plausibility of exploiting these effects to develop novel strategies against antibiotic
309 resistance.
310
311 **Materials and Methods**
312
313 Bacterial strains, media and growth conditions
314
315 All the strains used in this study (Data S1) derive from strains RB266, RB323 or RB324, which
316 are derivatives of *E. coli* K12 MG1655 (84). Fluorescently labeled strains harbor a copy of either
317 yellow fluorescent protein (YFP) or cyan fluorescent protein (CFP) under the control of the LacI-
318 regulated promoter P_{LacO-1} inserted either in the *yzgL* pseudogene locus or in the *galK* gene, a deletion
319 comprising the entire *lac* operon (to make constitutive the expression of the fluorescent proteins), and
320 the SOS reporter construction P_{sulA}-*mCherry* inserted in the *ysaCD* pseudogene locus. The SOS reporter
321 fusion was constructed by replacing a *tetA-sacB* selectable/counterselectable marker (85) located
322 upstream from a *mCherry-FRT-aph-FRT* cassette previously inserted in the *ysaCD* locus by the

323 regulatory regions (150bp upstream from the translation initiation site) of the SOS-regulated gene *sulA*.
324 Resistant mutants additionally carry different chromosomal alleles conferring antibiotic resistance. The
325 fluorescent constructions were generated by Lambda-Red recombineering (86–88), followed by
326 transference to a clean background by P1 transduction (89), and subsequent transduction of the
327 resistance alleles. The clean deletion of *rnhA* was constructed by markerless recombineering using a
328 *tetR-*P_{tet}*-ccdB-cat* selection/counterselection cassette as described by Figueroa-Bossi & Bossi (90), and
329 subsequent transfer of the markerless deletion to a clean background by P1 transduction, using as
330 recipient an isogenic strain carrying a deletion of the nearby gene *proB*, which causes proline
331 auxotrophy, and selecting for growth in minimal medium. The presence of each construction/mutation
332 was assessed by PCR-mediated amplification of the corresponding region and Sanger sequencing. The
333 Gam-GFP construction (49) was generously contributed by Professor Susan M. Rosenberg. The
334 chromosomal construction comprising a copy of the *rnhA* gene under the control of a promoter
335 inducible by arabinose (62) was kindly donated by Dr. Christian J. Rudolph. Derivatives of these
336 strains carrying the P_{sulA}*-mCherry* and different resistance mutations were constructed by P1
337 transduction. The plasmid pRB-5 (carrying the *rnhA* gene under the control of a promoter inducible by
338 anhydrotetracycline) was constructed by PCR amplification of the vector pZS*11 (91) and the
339 construction *tetR-*$P_{LTetO-1}$*-rnhA* from strain RB1207, subsequent restriction with AatII and HindIII
340 enzymes, ligation and electroporation. The construction *tetR-*$P_{LTetO-1}$*-rnhA* in strain RB1207 was made
341 by Lambda-Red recombineering (86–88), and selection/counterselection (85), over a previous $P_{LtetO-1}$-
342 *sfGFP* construction (92). The plasmids carrying an inducible copy of either *dksA* or *dnaA* were
343 obtained from the ASKA library of *E. coli* ORF clones (93). Cultures were grown in either Lysogeny
344 Broth (LB, Miller formulation) (94) or M9 broth supplemented with 0.4% glucose (95), in round-
345 bottom 96-well plates incubated at 37°C with shaking (700 r.p.m.) in a Grant-bio PHMP-4 benchtop
346 incubator, unless indicated otherwise. Solid medium was LB containing 1.5% agar. Media were
347 supplemented when necessary with antibiotics at the following concentrations: rifampicin (100 µg/ml),

348 streptomycin (100 µg/ml), ampicillin (100 µg/ml), erythromycin (150 µg/ml), kanamycin (100 µg/ml),
349 chloramphenicol (25 µg/ml).

350

351 Competitive fitness/SOS induction assays

352

353 The relative fitness (selection coefficient per generation) of each YFP-tagged resistant strain
354 carrying the SOS reporter was measured by competitive growth against a CFP-labeled isogenic
355 sensitive strain *E. coli* K12 MG1655 also carrying the SOS reporter. The formula used to calculate the
356 selection coefficient was $s=[\ln(NRf/NSf)-\ln(NRi/NSi)]\ln(NSf/NSi)$, being ***NRi*** and ***NRf*** the initial
357 and final number of resistant bacteria, and ***NSi*** and ***NSf*** the initial and final number of sensitive
358 bacteria. The competitor strains were first streaked out of their respective frozen vials, then individual
359 colonies were inoculated separately in medium without antibiotics and incubated overnight
360 (approximately 16h); the next morning, the number of cells in each culture was measured by Flow
361 Cytometry, and 10 µl of 1:1 mixtures of YFP and CFP bacteria were added to 140 µl of medium, at an
362 initial number of approximately 10^6 cells. The initial and final frequencies of the strains were obtained
363 by counting their cell numbers in the Flow Cytometer. The number of generations was estimated from
364 that of the reference strain (approximately five generations at 4h, and approximately eight generations
365 at 24h), and the selection coefficient was determined as described above for each independent
366 competition. The proportion of SOS-induced bacteria was quantified as the number of either YFP-
367 tagged or CFP-labeled bacteria showing red fluorescence (from the P_{sulA}-*mCherry* SOS reporter fusion)
368 above a threshold determined by the fluorescence levels of the control strains *lexA (ind-)* (constitutive
369 repression of the SOS response) and *ΔlexA* (constitutive activation of the SOS response) (96). The data
370 represented is the induction level of each mutant normalized with respect to the induction levels of the
371 sensitive it is competing against. In the competitions including the RNase HI inhibitor 2-[[[3-Bromo-5-

(2-furanyl)-7-(trifluoromethyl)pyrazolo[1,5-a]pyrimidin-2-yl]carbonyl]amino]-4,5,6,7-tetrahydro-benzo[b]thiophene-3-carboxylic acid ethyl ester (RHI001, Glixx Laboratories Inc., catalog number GLXC-03982), the medium was supplemented with 500 µM of RHI001, unless indicated otherwise.

Flow Cytometry

A BD LSR Fortessa™ SORP flow cytometer was used to quantify bacteria, using a 96-well plate High-Throughput Sampler (HTS) and SPHERO fluorescent spheres (AccuCount 2.0 µm blank particles), in order to accurately measure volumes. Bacterial numbers were calculated based on the counts of fluorescently labeled bacteria with respect the known number of beads added to a given volume. The instrument was equipped with a 488 nm laser used for scatter parameters and YFP detection, a 442 nm laser for CFP detection and a 561 nm laser for mCherry detection. Relative to optical configuration, CFP, YPF and mCherry were measured using bandpass filters in the range of 470/20 nm, 540/30 nm and 630/75nm, respectively. The analyzer is also equipped with a forward scatter (FSC) detector in a photomultiplier tube (PMT) to detect bacteria. The samples were acquired using FACSDiVa (version 6.2) software, and analyzed using FlowJo (version 10.0.7r2). All Flow Cytometry experiments were performed at the Flow Cytometry Facility of the Instituto Gulbenkian de Ciência (IGC), Oeiras, Portugal.

Selection for Erm^R bacteria

Fifteen independent colonies of sensitive bacteria were separately inoculated in LB in a 96-well plate, incubated at 37°C with shaking (700 r.p.m) for 7 hours, and 0.1ml of either independent culture was plated onto a LB agar plate supplemented with 150 µg/ml erythromycin, and incubated at 37°C for

396 5 days (Erm^R strains grow in the presence of erythromycin, albeit slowly). Colonies able to grow in
397 these plates were streaked onto plates supplemented with 150 µg/ml erythromycin, in order to further
398 assess their *bona fide* resistance, and the *rplD*, and *rplV* genes of the resistant clones were amplified by
399 PCR and analyzed by Sanger sequencing.
400

401 Microscopy

402

403 Early exponential cultures were diluted into pre-warmed medium containing the inducer of the
404 Gam-GFP construction (anhydrotetracycline, 25 ng/ml) and incubated at 37°C with shaking (240
405 r.p.m.) for 3h, prior to imaging. Bacterial solutions were then placed onto 1% agarose (in 1X PBS) pads
406 mounted in adhesive frames between the microscope slide and a coverglass. Images were acquired on
407 an Applied Precision DeltavisionCORE system, mounted on an Olympus IX71 inverted microscope,
408 coupled to a Cascade II 1024x1024 EM-CCD camera, using an Olympus 100x 1.4NA Uplan SAPO Oil
409 immersion objective, where GFP and mCherry were imaged with FITC (Ex: 475/28, EM: 528/38) and
410 TRITC (Ex: 542/28, Em: 617/73) fluorescence filter sets, respectively, and DIC optics. Images were
411 deconvoluted with Applied Precision's softWorx software, and prepared for presentation (cropping
412 smaller fields to facilitate visualization, and false-coloring green and red fluorescent signals) using
413 Fiji/ImageJ. All microscopy experiments were performed at the Imaging Facility of the IGC.

414

415 Spot assays

416

417 Sensitive and $RpsL^{K43N}$ $RpoB^{H526Y}$ strains carrying the expression vector pCA24N -gfp, either
418 empty or carrying the *dnaA* gene (93) were streaked individually onto LB agar plates supplemented

419 with the appropriate antibiotic (to select for the presence of the plasmid), and incubated overnight at
420 37°C. The next day, three independent colonies from each strain were inoculated separately in LB
421 broth supplemented with the appropriate antibiotic (150 µl per well) in a 96-well plate and incubated
422 overnight at 37°C with shaking (700 r.p.m). The next day, the OD_{600} of the overnight cultures was
423 measured using a Thermo Scientific Multiskan Go spectrophotometer, bacteria were appropriately
424 diluted in 1X PBS to generate solutions containing approximately 10^{10}, 10^{9}, 10^{8}, 10^{7}, 10^{6}, 10^{5}, 10^{4} or 10^{3}
425 cells/ml. Then 5 µl aliquots of these bacterial solutions (approximately $5x10^{7}$ to 5 cells) were spotted
426 onto LB agar plates supplemented with the appropriate antibiotic (to select for the presence of the
427 plasmid) and either 0 or 50 µM Isopropyl ß-D-1-thiogalactopyranoside (IPTG) and incubated overnight
428 at 37°C. Each experiment included three biological replicates and three experiments were performed;
429 representative data sets are shown.
430

431 Long-term propagations of polymorphic populations

432

433 The CFP-tagged sensitive (either WT or *ΔrnhA*) and the five YFP-labeled resistant bacteria
434 (either $RpsL^{K43N}$, $RpsL^{K43T}$, $RpoB^{H526L}$, $RpoB^{H526Y}$, and $RpoB^{S531F}$ or *ΔrnhA* $RpsL^{K43N}$, *ΔrnhA* $RpsL^{K43T}$,
435 *ΔrnhA* $RpoB^{H526L}$, *ΔrnhA* $RpoB^{H526Y}$, and *ΔrnhA* $RpoB^{S531F}$) were streaked individually onto LB agar
436 plates and incubated overnight at 37°C. The next day, three independent colonies from each strain were
437 inoculated separately in LB broth (150 µl per well) in a 96-well plate and incubated overnight at 37°C
438 with shaking (700 r.p.m). The next day, bacteria were quantified by Flow Cytometry, and 10 µl of
439 1:1:1:1:1:1 mixtures of the sensitive and either resistant bacteria were added to 140 µl of medium, at an
440 initial number of approximately 10^{6} cells. The initial frequencies of the fluorescent strains were
441 confirmed by Flow Cytometry. Every 24h, during 15 days, bacterial cultures were diluted in 1X PBS
442 by a factor of 10^{-2}, then 10 µl of these diluted cultures were transferred to 140 µl fresh LB broth and

allowed to grow for additional 24h, reaching approximately 10^9 cells/ml. In parallel, cell numbers were counted using the Flow Cytometer, in order to measure the frequency of each strain in the mixed population during the experiment, by collecting a sample (10 µl) from the spent culture each day.

Growth curves

In the experiments involving RHI001, YFP-tagged sensitive and $RpsL^{K43N}$ $RpoB^{H526Y}$ strains were streaked individually onto LB agar plates and incubated overnight at 37°C. The next day, three independent colonies from each strain were inoculated separately in LB broth (150 µl per well) in a 96-well plate and incubated overnight at 37°C with shaking (700 r.p.m). The next day, bacteria were quantified by Flow Cytometry, and approximately $5x10^5$ bacteria were inoculated in 100-well plates containing LB broth supplemented with either 0.5% DMSO (the solvent of RHI001) or 50 µM RHI001 (150 µl per well), and incubated at 37ºC with continuous shaking (medium amplitude, duration 5s, 10s interval, and stopping 5s before each measurement) in a Bioscreen C (Oy Growth Curves Ab Ltd.) benchtop microplate reader, measuring OD_{600} every 30 minutes during 12h. In the experiments involving sensitive and $RpsL^{K43N}$ $RpoB^{H526Y}$ strains carrying the expression vector pCA24N -gfp, either empty or carrying the gene *dksA* (93), the strains were streaked individually onto LB agar plates supplemented with the appropriate antibiotic (to select for the presence of the plasmid), and incubated overnight at 37°C. The next day, three independent colonies from each strain were inoculated separately in LB broth supplemented with the appropriate antibiotic (150 µl per well) in a 96-well plate and incubated overnight at 37°C with shaking (700 r.p.m). The next day, the OD_{600} of the overnight cultures was measured using a Thermo Scientific Multiskan Go spectrophotometer, bacteria were appropriately diluted in 1X PBS, and approximately $5x10^5$ bacteria were inoculated in flat-bottom 96-well plates containing LB broth (150 µl per well) supplemented with the appropriate antibiotic and either 0 or 50 µM IPTG, and incubated at 37ºC (1ºC up to bottom gradient, “lid on” option) with

468 double orbital shaking (set as "fast") in a Biotek SYNERGY H1 benchtop microplate reader,
469 measuring OD_{600} every 30 minutes during 24h.
470
471 Animal experiments
472
473 Adult C57BL/6J female mice (six to eight weeks old) were kept in ventilated cages under
474 specified pathogen free (SPF) barrier conditions at the animal facility of the IGC. To overcome
475 bacterial colonization resistance, mice were treated with streptomycin (5 g/L) in drinking water during
476 seven days and then put on regular autoclaved water for two days to wash out the antibiotic from the
477 intestine. The following day, animals were deprived of food and water during the 4 hours prior to
478 inoculation by oral gavage of 100 µl of bacterial suspension containing ~10^9 cells. All animals were
479 then individually-caged, with food and water being available *ad libitum*. Each animal (6 per group) was
480 gavaged with a mix (9:1) of CFP-tagged sensitive (either WT or *ΔrnhA*) and YFP-labeled double
481 resistant bacteria (either $RpsL^{K43T}$ $RpoB^{H526Y}$ or *ΔrnhA* $RpsL^{K43T}$ $RpoB^{H526Y}$). In order to obtain the
482 bacterial suspensions, the strains were streaked individually onto appropriate antibiotic-supplemented
483 LB agar plates and incubated overnight at 37°C. The next day, three independent colonies from each
484 strain were inoculated separately in assay tubes containing 5ml of BHI broth supplemented with the
485 appropriate antibiotic and bacterial cultures were grown overnight at 37°C with shaking (240 r.p.m).
486 The next day, each bacterial culture was diluted 100-fold (20 µl of overnight culture in 2 ml of fresh
487 BHI broth, in 125 ml flasks) and incubated at 37°C with shaking (240 r.p.m) until reaching an $OD_{600} \approx$
488 2. Then the cultures were washed once with 1X PBS and Flow cytometry was used to assess the
489 appropriate cells numbers and prepare bacterial mixes for gavage. Mouse fecal pellets were collected at
490 8 hours after gavage, and afterwards on a daily basis during 13 days, to analyze the loads and frequency
491 of each strain colonizing the gut along time. Fecal samples were stored in 15% glycerol at -80°C. In
492 order to measure the loads (CFUs/g of feces) and the frequency of each strain along the experiment,

fecal samples were plated on appropriate antibiotic-supplemented plates and incubated overnight to assess CFUs of CFP- or YFP-labeled bacteria using a SteREOLumar Carl Zeiss fluorescent stereoscope. Every strain that remained below the detection limit (~10^2 CFUs/g of feces) for three consecutive time points was considered extinct. For the post-gavage antibiotic treatment, streptomycin (5 g/L) was dispensed in drinking water during seven days. The animal experiments included in this work were reviewed and approved by both the Ethics Committee and the Animal Welfare Body of the IGC (license A009.2018) and by the Direção Geral de Alimentação e Veterinária (DGAV, Portuguese national entity that regulates the use of laboratory animals; license 009676). All experiments conducted on animals followed the Portuguese (Decreto-Lei nº 113/2013) and European (Directive 2010/63/EU) legislations concerning housing, husbandry and animal welfare.

Statistical analyses

All analyses were conducted using Libreoffice Calc version 5.4.1.2 (www.libreoffice.org) software, R version 3.4.4 (www.r-project.org) software via RStudio version 1.1.442 interface (www.rstudio.com) and GraphPad Prism version 7.04 (www.graphpad.com). For each set of competitions ($n \geq 3$), two-tailed unpaired Student's *t*-tests were used. For testing the association between the fitness cost and the level of SOS induction, a linear regression of the selection coefficient (s) with the logarithm of the fold change in SOS induction of each resistant clone (with respect to the sensitive bacteria it is competing against in the same well), was used.

Acknowledgements

The authors thank Professor Susan M. Rosenberg and Dr. Christian J. Rudolph for kindly providing bacterial strains, the Flow Cytometry and Advanced Imaging facilities of Instituto Gulbenkian de Ciência for technical assistance, Miguel Godinho for useful discussions, and Jonathan Howard, Karina Xavier, Leonardo Gastón Guilgur, Pol Nadal Jiménez and the members of the Gordo and Xavier labs for critically reading earlier versions of this manuscript. This work was funded by the the Marie Sklodowska-Curie Actions (MSCA) with the fellowship 746690-ResistEpist-H2020-MSCA-IF-2016/H2020-MSCA-IF-2016, to R.B., and partially supported by the PREPARE project (JPIAMR/0001/2016-ERA NET), and by ONEIDA and Congento projects (LISBOA-01-0145-FEDER-016417 and LISBOA-01-0145-FEDER-022170), both co-funded by FEEI - "Fundos Europeus Estruturais e de Investimento" from "Programa Operacional Regional Lisboa 2020", and by national funds from "Fundação para a Ciência e a Tecnologia" (FCT), to I.G. R.B. was also supported by the FCT with the fellowship SFRH/BDP/109517/2015. The authors declare no conflicts of interest.

Author contributions

R.B: conceptualization, formal analysis, funding acquisition, investigation, methodology, visualization, writing – original draft. N.F: formal analysis, investigation, methodology, writing – review & editing. I.G: conceptualization, formal analysis, funding acquisition, methodology, project administration, resources, supervision, writing – review & editing.

Competing interests

The authors declare no competing interests.

Data availability

All the strains used (Data S1) are available via Material Transfer Agreement (MTA). The raw data of the experiments shown in all figures and the table are available in Data S2. The images analyzed to obtain the data shown in Table 1, and those used in Figures S1 and S3 are available in the public data repository Zenodo (DOI: 10.5281/zenodo.3381746).

References

1. Global antimicrobial resistance surveillance system (GLASS) report: early implementation 2017-2018. Geneva: World Health Organization. 2018.

2. Durão P, Balbontín R, Gordo I. Evolutionary Mechanisms Shaping the Maintenance of Antibiotic Resistance. Trends Microbiol. 2018;26(8):677–91.

3. Andersson DI, Hughes D. Antibiotic resistance and its cost: is it possible to reverse resistance? Nat Rev Microbiol. 2010 Apr;8(4):260–71.

4. Vogwill T, MacLean RC. The genetic basis of the fitness costs of antimicrobial resistance: a meta-analysis approach. Evol Appl. 2015 Mar;8(3):284–95.

5. Andersson DI, Levin BR. The biological cost of antibiotic resistance. Curr Opin Microbiol. 1999 Oct;2(5):489–93.

6. Eliopoulos GM. Aminoglycoside resistant enterococcal endocarditis. Infect Dis Clin North Am. 1993 Mar;7(1):117–33.

7. Goldstein BP. Resistance to rifampicin: a review. J Antibiot (Tokyo). 2014 Sep;67(9):625–30.

8. Lemos ACM, Matos ED. Multidrug-resistant tuberculosis. Braz J Infect Dis Off Publ Braz Soc Infect Dis. 2013 Apr;17(2):239–46.

9. Jin DJ, Gross CA. Characterization of the pleiotropic phenotypes of rifampin-resistant rpoB mutants of Escherichia coli. J Bacteriol. 1989 Sep;171(9):5229–31.

10. Reynolds MG. Compensatory evolution in rifampin-resistant Escherichia coli. Genetics. 2000 Dec;156(4):1471–81.

11. Das A, Merril C, Adhya S. Interaction of RNA polymerase and rho in transcription termination: coupled ATPase. Proc Natl Acad Sci U S A. 1978 Oct;75(10):4828–32.

12. Fisher RF, Yanofsky C. Mutations of the beta subunit of RNA polymerase alter both transcription pausing and transcription termination in the trp operon leader region in vitro. J Biol Chem. 1983 Jul 10;258(13):8146–50.

13. Gowrishankar J, Pittard J. Regulation of phenylalanine biosynthesis in Escherichia coli K-12: control of transcription of the pheA operon. J Bacteriol. 1982 Jun;150(3):1130–7.

14. Guarente LP, Beckwith J. Mutant RNA polymerase of Escherichia coli terminates transcription in strains making defective rho factor. Proc Natl Acad Sci U S A. 1978 Jan;75(1):294–7.

15. Hammer K, Jensen KF, Poulsen P, Oppenheim AB, Gottesman M. Isolation of Escherichia coli rpoB mutants resistant to killing by lambda cII protein and altered in pyrE gene attenuation. J Bacteriol. 1987 Nov;169(11):5289–97.

16. Jin DJ, Gross CA. RpoB8, a rifampicin-resistant termination-proficient RNA polymerase, has an increased Km for purine nucleotides during transcription elongation. J Biol Chem. 1991 Aug 5;266(22):14478–85.

17. Jin DJ, Walter WA, Gross CA. Characterization of the termination phenotypes of rifampicin-resistant mutants. J Mol Biol. 1988 Jul 20;202(2):245–53.

18. Jin DJ, Cashel M, Friedman DI, Nakamura Y, Walter WA, Gross CA. Effects of rifampicin resistant rpoB mutations on antitermination and interaction with nusA in Escherichia coli. J Mol Biol. 1988 Nov 20;204(2):247–61.

19. Reynolds MG. Compensatory evolution in rifampin-resistant Escherichia coli. Genetics. 2000 Dec;156(4):1471–81.

20. Yanofsky C, Horn V. Rifampin resistance mutations that alter the efficiency of transcription termination at the tryptophan operon attenuator. J Bacteriol. 1981 Mar;145(3):1334–41.

21. Zhou YN, Jin DJ. RNA polymerase beta mutations have reduced sigma70 synthesis leading to a hyper-temperature-sensitive phenotype of a sigma70 mutant. J Bacteriol. 1997 Jul;179(13):4292–8.

22. Zhou YN, Jin DJ. The rpoB mutants destabilizing initiation complexes at stringently controlled promoters behave like “stringent” RNA polymerases in Escherichia coli. Proc Natl Acad Sci U S A. 1998 Mar 17;95(6):2908–13.

23. Zhou YN, Lubkowska L, Hui M, Court C, Chen S, Court DL, et al. Isolation and characterization of RNA polymerase rpoB mutations that alter transcription slippage during elongation in Escherichia coli. J Biol Chem. 2013 Jan 25;288(4):2700–10.

24. Paulander W, Maisnier-Patin S, Andersson DI. The fitness cost of streptomycin resistance depends on rpsL mutation, carbon source and RpoS (sigmaS). Genetics. 2009 Oct;183(2):539–46, 1SI-2SI.

25. Ruusala T, Andersson D, Ehrenberg M, Kurland CG. Hyper-accurate ribosomes inhibit growth. EMBO J. 1984 Nov;3(11):2575–80.

26. Schrag SJ, Perrot V. Reducing antibiotic resistance. Nature. 1996 May 9;381(6578):120–1.

27. Birge EA, Kurland CG. Altered ribosomal protein in streptomycin-dependent Escherichia coli. Science. 1969 Dec 5;166(3910):1282–4.

28. Bohman K, Ruusala T, Jelenc PC, Kurland CG. Kinetic impairment of restrictive streptomycin-resistant ribosomes. Mol Gen Genet MGG. 1984;198(2):90–9.

29. Dong H, Kurland CG. Ribosome mutants with altered accuracy translate with reduced processivity. J Mol Biol. 1995 May 5;248(3):551–61.

30. Galas DJ, Branscomb EW. Ribosome slowed by mutation to streptomycin resistance. Nature. 1976 Aug 12;262(5569):617–9.

31. Gartner TK, Orias E. Effects of mutations to streptomycin resistance on the rate of translation of mutant genetic information. J Bacteriol. 1966 Mar;91(3):1021–8.

32. Gorini L, Kataja E. STREPTOMYCIN-INDUCED OVERSUPPRESSION IN E. COLI. Proc Natl Acad Sci U S A. 1964 Jun;51:995–1001.

33. McMahon G, Landau JV. Effect of S12 ribosomal mutations on peptide chain elongation in Escherichia coli: a hydrostatic pressure study. J Bacteriol. 1982 Jul;151(1):516–20.

34. Ozaki M, Mizushima S, Nomura M. Identification and functional characterization of the protein controlled by the streptomycin-resistant locus in E. coli. Nature. 1969 Apr 26;222(5191):333–9.

35. Applebee MK, Herrgård MJ, Palsson BØ. Impact of individual mutations on increased fitness in adaptively evolved strains of Escherichia coli. J Bacteriol. 2008 Jul;190(14):5087–94.

36. Hall AR, Iles JC, MacLean RC. The fitness cost of rifampicin resistance in Pseudomonas aeruginosa depends on demand for RNA polymerase. Genetics. 2011 Mar;187(3):817–22.

37. Qi Q, Preston GM, MacLean RC. Linking system-wide impacts of RNA polymerase mutations to the fitness cost of rifampin resistance in Pseudomonas aeruginosa. mBio. 2014 Dec 9;5(6):e01562.

38. Ochi K, Hosaka T. New strategies for drug discovery: activation of silent or weakly expressed microbial gene clusters. Appl Microbiol Biotechnol. 2013 Jan;97(1):87–98.

39. Pelchovich G, Nadejda S, Dana A, Tuller T, Bravo IG, Gophna U. Ribosomal mutations affecting the translation of genes that use non-optimal codons. FEBS J. 2014 Aug;281(16):3701–18.

40. Moura de Sousa J, Balbontín R, Durão P, Gordo I. Multidrug-resistant bacteria compensate for the epistasis between resistances. PLoS Biol. 2017;15(4):e2001741.

41. Burmann BM, Schweimer K, Luo X, Wahl MC, Stitt BL, Gottesman ME, et al. A NusE:NusG complex links transcription and translation. Science. 2010 Apr 23;328(5977):501–4.

42. Dutta D, Shatalin K, Epshtein V, Gottesman ME, Nudler E. Linking RNA polymerase backtracking to genome instability in E. coli. Cell. 2011 Aug 19;146(4):533–43.

43. Herbert KM, Zhou J, Mooney RA, Porta AL, Landick R, Block SM. E. coli NusG inhibits backtracking and accelerates pause-free transcription by promoting forward translocation of RNA polymerase. J Mol Biol. 2010 May 28;399(1):17–30.

44. Kohler R, Mooney RA, Mills DJ, Landick R, Cramer P. Architecture of a transcribing-translating expressome. Science. 2017 14;356(6334):194–7.

45. Proshkin S, Rahmouni AR, Mironov A, Nudler E. Cooperation between translating ribosomes and RNA polymerase in transcription elongation. Science. 2010 Apr 23;328(5977):504–8.

46. Saxena S, Myka KK, Washburn R, Costantino N, Court DL, Gottesman ME. Escherichia coli transcription factor NusG binds to 70S ribosomes. Mol Microbiol. 2018;108(5):495–504.

47. Maslowska KH, Makiela-Dzbenska K, Fijalkowska IJ. The SOS system: A complex and tightly regulated response to DNA damage. Environ Mol Mutagen. 2019;60(4):368–84.

48. Quillardet P, Huisman O, D'Ari R, Hofnung M. SOS chromotest, a direct assay of induction of an SOS function in Escherichia coli K-12 to measure genotoxicity. Proc Natl Acad Sci U S A. 1982 Oct;79(19):5971–5.

49. Shee C, Cox BD, Gu F, Luengas EM, Joshi MC, Chiu L-Y, et al. Engineered proteins detect spontaneous DNA breakage in human and bacterial cells. eLife. 2013 Oct 29;2:e01222.

50. Sedlyarova N, Rescheneder P, Magán A, Popitsch N, Rziha N, Bilusic I, et al. Natural RNA Polymerase Aptamers Regulate Transcription in E. coli. Mol Cell. 2017 Jul 6;67(1):30-43.e6.

51. Chittum HS, Champney WS. Ribosomal protein gene sequence changes in erythromycin-resistant mutants of Escherichia coli. J Bacteriol. 1994 Oct;176(20):6192–8.

52. Zaman S, Fitzpatrick M, Lindahl L, Zengel J. Novel mutations in ribosomal proteins L4 and L22 that confer erythromycin resistance in Escherichia coli. Mol Microbiol. 2007 Nov;66(4):1039–50.

53. Myka KK, Gottesman ME. DksA and DNA double-strand break repair. Curr Genet. 2019 Dec;65(6):1297–300.

54. Myka KK, Küsters K, Washburn R, Gottesman ME. DksA-RNA polymerase interactions support new origin formation and DNA repair in Escherichia coli. Mol Microbiol. 2019;111(5):1382–97.

55. Merrikh H, Zhang Y, Grossman AD, Wang JD. Replication-transcription conflicts in bacteria. Nat Rev Microbiol. 2012 Jun 6;10(7):449–58.

56. Merrikh H, Machón C, Grainger WH, Grossman AD, Soultanas P. Co-directional replication-transcription conflicts lead to replication restart. Nature. 2011 Feb 24;470(7335):554–7.

57. Wang CH, Koch AL. Constancy of growth on simple and complex media. J Bacteriol. 1978 Dec;136(3):969–75.

58. Skarstad K, Løbner-Olesen A, Atlung T, von Meyenburg K, Boye E. Initiation of DNA replication in Escherichia coli after overproduction of the DnaA protein. Mol Gen Genet MGG. 1989 Jul;218(1):50–6.

59. Lang KS, Hall AN, Merrikh CN, Ragheb M, Tabakh H, Pollock AJ, et al. Replication-Transcription Conflicts Generate R-Loops that Orchestrate Bacterial Stress Survival and Pathogenesis. Cell. 2017 Aug 10;170(4):787-799.e18.

60. Gan W, Guan Z, Liu J, Gui T, Shen K, Manley JL, et al. R-loop-mediated genomic instability is caused by impairment of replication fork progression. Genes Dev. 2011 Oct 1;25(19):2041–56.

61. Tadokoro T, Kanaya S. Ribonuclease H: molecular diversities, substrate binding domains, and catalytic mechanism of the prokaryotic enzymes. FEBS J. 2009 Mar;276(6):1482–93.

62. Stockum A, Lloyd RG, Rudolph CJ. On the viability of Escherichia coli cells lacking DNA topoisomerase I. BMC Microbiol. 2012 Feb 28;12:26.

63. Wimberly H, Shee C, Thornton PC, Sivaramakrishnan P, Rosenberg SM, Hastings PJ. R-loops and nicks initiate DNA breakage and genome instability in non-growing Escherichia coli. Nat Commun. 2013;4:2115.

64. Tramontano E, Corona A, Menendez-Arias L. Ribonuclease H, an unexploited target for antiviral intervention against HIV and hepatitis B virus. Antiviral Res. 2019 Sep 21;104613.

65. Kim J, Yoon J, Ju M, Lee Y, Kim T-H, Kim J, et al. Identification of two HIV inhibitors that also inhibit human RNaseH2. Mol Cells. 2013 Sep;36(3):212–8.

66. Melnyk AH, Wong A, Kassen R. The fitness costs of antibiotic resistance mutations. Evol Appl. 2015 Mar;8(3):273–83.

67. Sousa A, Frazão N, Ramiro RS, Gordo I. Evolution of commensal bacteria in the intestinal tract of mice. Curr Opin Microbiol. 2017 Aug;38:114–21.

68. Cardoso LL, Durão P, Amicone M, Gordo I. Dysbiosis personalizes fitness effect of antibiotic resistance in the mammalian gut. bioRxiv. 2019 Aug 28;748897.

69. Hosaka T, Tamehiro N, Chumpolkulwong N, Hori-Takemoto C, Shirouzu M, Yokoyama S, et al. The novel mutation K87E in ribosomal protein S12 enhances protein synthesis activity during the late growth phase in Escherichia coli. Mol Genet Genomics MGG. 2004 Apr;271(3):317–24.

70. Trindade S, Sousa A, Xavier KB, Dionisio F, Ferreira MG, Gordo I. Positive epistasis drives the acquisition of multidrug resistance. PLoS Genet. 2009 Jul;5(7):e1000578.

71. Broccoli S, Rallu F, Sanscartier P, Cerritelli SM, Crouch RJ, Drolet M. Effects of RNA polymerase modifications on transcription-induced negative supercoiling and associated R-loop formation. Mol Microbiol. 2004 Jun;52(6):1769–79.

72. Negro V, Krin E, Aguilar Pierlé S, Chaze T, Giai Gianetto Q, Kennedy SP, et al. RadD Contributes to R-Loop Avoidance in Sub-MIC Tobramycin. mBio. 2019 Jul 2;10(4).

73. Tehranchi AK, Blankschien MD, Zhang Y, Halliday JA, Srivatsan A, Peng J, et al. The transcription factor DksA prevents conflicts between DNA replication and transcription machinery. Cell. 2010 May 14;141(4):595–605.

74. Durão P, Trindade S, Sousa A, Gordo I. Multiple Resistance at No Cost: Rifampicin and Streptomycin a Dangerous Liaison in the Spread of Antibiotic Resistance. Mol Biol Evol. 2015 Oct;32(10):2675–80.

75. Trindade S, Sousa A, Gordo I. Antibiotic resistance and stress in the light of Fisher's model. Evol Int J Org Evol. 2012 Dec;66(12):3815–24.

76. Katz S, Hershberg R. Elevated mutagenesis does not explain the increased frequency of antibiotic resistant mutants in starved aging colonies. PLoS Genet. 2013 Nov;9(11):e1003968.

77. Wrande M, Roth JR, Hughes D. Accumulation of mutants in "aging" bacterial colonies is due to growth under selection, not stress-induced mutagenesis. Proc Natl Acad Sci U S A. 2008 Aug 19;105(33):11863–8.

78. Kogoma T. Stable DNA replication: interplay between DNA replication, homologous recombination, and transcription. Microbiol Mol Biol Rev MMBR. 1997 Jun;61(2):212–38.

79. Quiñones A, Kücherer C, Piechocki R, Messer W. Reduced transcription of the rnh gene in Escherichia coli mutants expressing the SOS regulon constitutively. Mol Gen Genet MGG. 1987 Jan;206(1):95–100.

80. Hershberg R. Antibiotic-Independent Adaptive Effects of Antibiotic Resistance Mutations. Trends Genet TIG. 2017;33(8):521–8.

81. Almeida Da Silva PEA, Palomino JC. Molecular basis and mechanisms of drug resistance in Mycobacterium tuberculosis: classical and new drugs. J Antimicrob Chemother. 2011 Jul;66(7):1417–30.

82. Gupta R, Chatterjee D, Glickman MS, Shuman S. Division of labor among Mycobacterium smegmatis RNase H enzymes: RNase H1 activity of RnhA or RnhC is essential for growth whereas RnhB and RnhA guard against killing by hydrogen peroxide in stationary phase. Nucleic Acids Res. 2017 09;45(1):1–14.

83. Minias AE, Brzostek AM, Korycka-Machala M, Dziadek B, Minias P, Rajagopalan M, et al. RNase HI Is Essential for Survival of Mycobacterium smegmatis. PloS One. 2015;10(5):e0126260.

84. Blattner FR, Plunkett G, Bloch CA, Perna NT, Burland V, Riley M, et al. The complete genome sequence of Escherichia coli K-12. Science. 1997 Sep 5;277(5331):1453–62.

85. Li X-T, Thomason LC, Sawitzke JA, Costantino N, Court DL. Positive and negative selection using the tetA-sacB cassette: recombineering and P1 transduction in Escherichia coli. Nucleic Acids Res. 2013 Dec;41(22):e204.

86. Datsenko KA, Wanner BL. One-step inactivation of chromosomal genes in Escherichia coli K-12 using PCR products. Proc Natl Acad Sci U S A. 2000 Jun 6;97(12):6640–5.

87. Murphy KC, Campellone KG, Poteete AR. PCR-mediated gene replacement in Escherichia coli. Gene. 2000 Apr 4;246(1–2):321–30.

88. Yu D, Ellis HM, Lee EC, Jenkins NA, Copeland NG, Court DL. An efficient recombination system for chromosome engineering in Escherichia coli. Proc Natl Acad Sci U S A. 2000 May 23;97(11):5978–83.

89. Lennox ES. Transduction of linked genetic characters of the host by bacteriophage P1. Virology. 1955 Jul;1(2):190–206.

90. Figueroa-Bossi N, Bossi L. Recombineering applications for the mutational analysis of bacterial RNA-binding proteins and their sites of action. Methods Mol Biol Clifton NJ. 2015;1259:103–16.

91. Subramaniam AR, Pan T, Cluzel P. Environmental perturbations lift the degeneracy of the genetic code to regulate protein levels in bacteria. Proc Natl Acad Sci U S A. 2013 Feb 5;110(6):2419–24.

92. Balbontín R, Vlamakis H, Kolter R. Mutualistic interaction between Salmonella enterica and Aspergillus niger and its effects on Zea mays colonization. Microb Biotechnol. 2014 Nov;7(6):589–600.

93. Kitagawa M, Ara T, Arifuzzaman M, Ioka-Nakamichi T, Inamoto E, Toyonaga H, et al. Complete set of ORF clones of Escherichia coli ASKA library (a complete set of E. coli K-12 ORF archive): unique resources for biological research. DNA Res Int J Rapid Publ Rep Genes Genomes. 2005;12(5):291–9.

94. Bertani G. Studies on lysogenesis. I. The mode of phage liberation by lysogenic Escherichia coli. J Bacteriol. 1951 Sep;62(3):293–300.

95. Maniatis et al. Molecular cloning: a laboratory manual (CSHL Press).

96. Lin LL, Little JW. Isolation and characterization of noncleavable (Ind-) mutants of the LexA repressor of Escherichia coli K-12. J Bacteriol. 1988 May;170(5):2163–73.

Figures

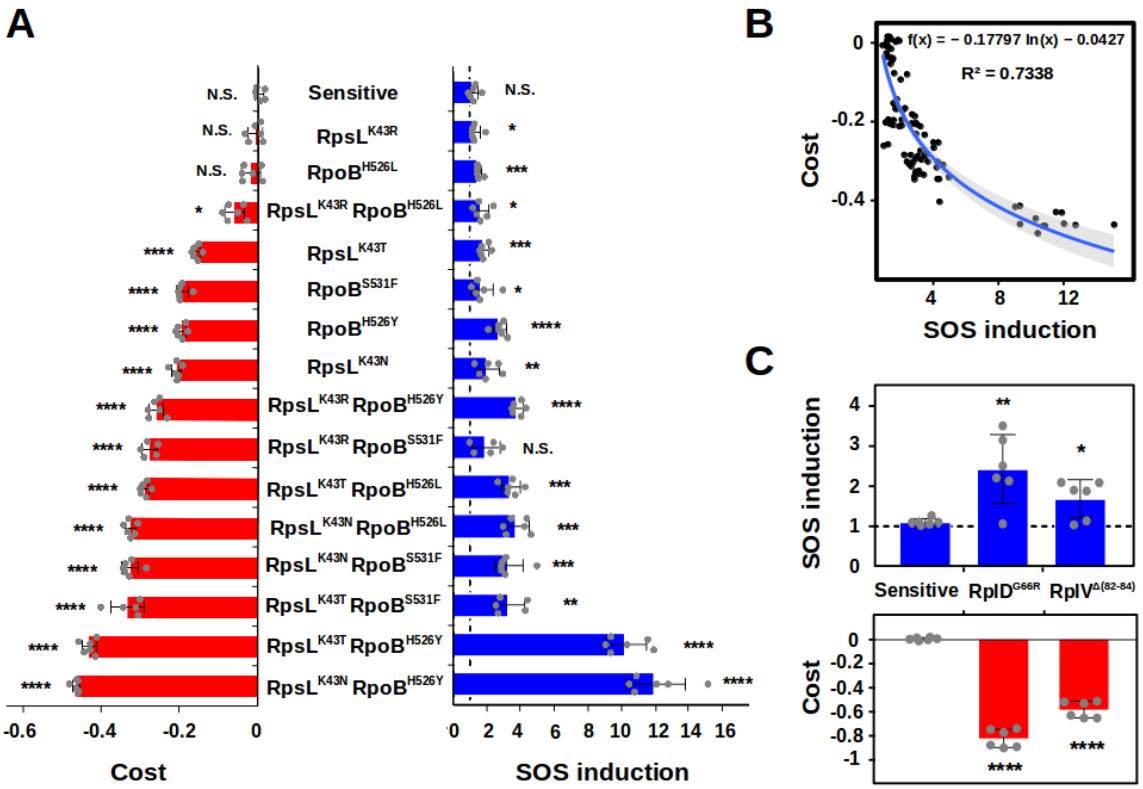

Figure 1. DNA breaks explain variation in the fitness cost of resistance. A. Fitness cost (red bars) and SOS induction (blue bars) of sensitive bacteria and Str^R and Rif^R mutants in LB broth at 4 hours. The strains are ordered from lower to higher fitness cost (top to bottom). The dashed line indicates no SOS induction. Error bars represent mean ± standard deviation of independent biological replicates (n≥5). N.S. non-significant; **P* < 0.05; ***P* < 0.01; ****P* < 0.001; *****P* < 0.0001 (two-tailed Student's *t* test). **B.** Correlation between the fitness cost (y axis) and the SOS induction (x axis) representing all the data points from A. The blue line represents the logarithmic regression line, and the grey area represents the 95% confidence interval. **C.** SOS induction (blue bars) and fitness cost (red bars) of sensitive bacteria and Erm^R mutants in LB broth at 4 hours. The dashed line indicates no SOS induction. Error bars represent mean ± standard deviation of independent biological replicates (n=6). N.S. non-significant; **P* < 0.05; ***P* < 0.01; ****P* < 0.001; *****P* < 0.0001 (two-tailed Student's *t* test).

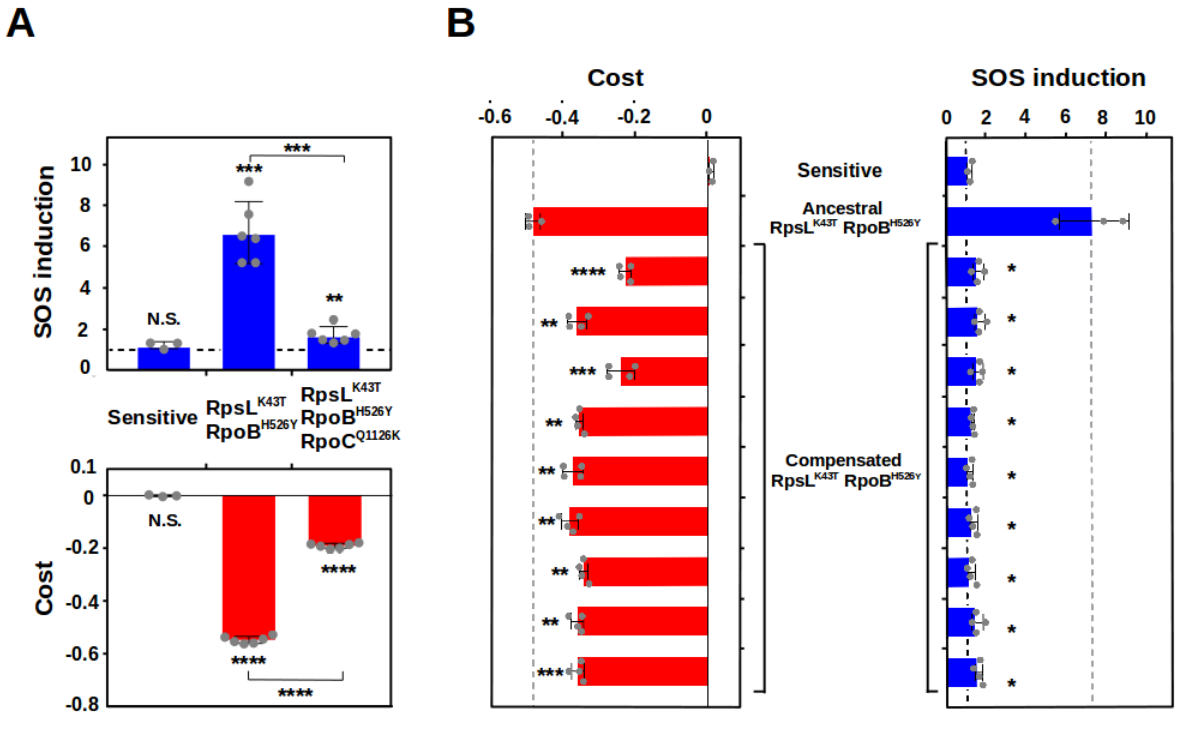

Figure 2. Compensatory evolution cause reduction of DNA breaks. A. SOS induction (blue bars) and fitness cost (red bars), of sensitive (left) double resistant (center) and double resistant carrying a compensatory mutation (right) bacteria in LB broth at 4 hours. The dashed line indicates no SOS induction. Error bars represent mean ± standard deviation of independent biological replicates (n≥3). N.S. non-significant; **P* < 0.05; ***P* < 0.01; ****P* < 0.001; *****P* < 0.0001 (two-tailed Student's *t* test). **B.** Fitness cost (red bars), and SOS induction (blue bars) of sensitive, ancestral $RpsL^{K43T}$ $RpoB^{H526Y}$ and nine compensated clones in LB broth at 4 hours. The black dashed line indicates no SOS induction. The grey dashed lines mark the cost/SOS of the ancestral double mutant. Error bars represent mean ± standard deviation of independent biological replicates (n≥3). N.S. non-significant; **P* < 0.05; ***P* < 0.01; ****P* < 0.001; *****P* < 0.0001 (two-tailed Student's *t* test).

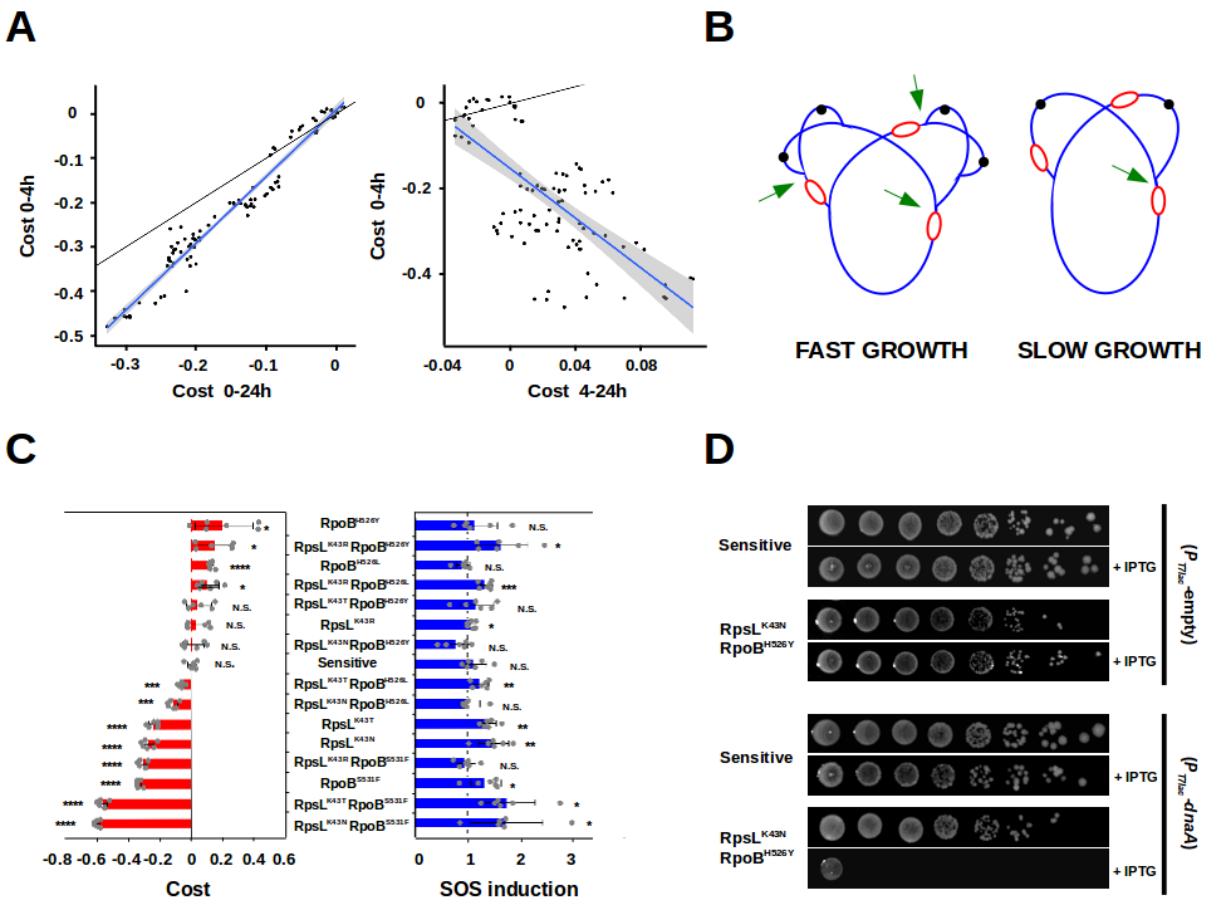

Figure 3. Replication speed affects the cost of resistance. A. Left panel: correlation of the fitness cost between time 0 and 4h (y axis) and between time 0 and 24h (y axis), in LB broth. Right panel: correlation of the fitness cost between time 0 and 4h (y axis) and between time 4h and 24h (y axis), in LB broth. Black lines represent the linear regressions if the costs were identical. Blue lines represent the regression lines, and the grey areas represent the 95% confidence intervals. Data from the experiments shown in Figure 1A. **B**. Schematic representation of DNA replication of *E. coli* during fast (left) or slow (right) growth. Black dots represent the origin of replication, and red lines represent transcription forks; green arrows mark regions of potential replication-transcription conflicts. **C.** Fitness cost (red bars), and SOS induction (blue bars) of sensitive bacteria and Str^R and/or Rif^R mutants in minimal medium at 8 hours. The strains are ordered from lower to higher cost (top to bottom). The dashed line indicates no SOS induction. Error bars represent mean ± standard deviation of independent biological replicates (n=6). N.S. non-significant; $*P < 0.05$; $**P < 0.01$; $***P < 0.001$; $****P < 0.0001$ (two-tailed Student's *t* test). **D.** Aliquots of serial dilutions (approximately from $5x10^7$ to 5 cells) of sensitive and $RpsL^{K43N}$ $RpoB^{H526Y}$ strains carrying the expression vector pCA24N -gfp, either empty (top, strains RB1317 and RB1321) or harboring the gene *dnaA* (bottom, strains RB1290 and RB1294) and either in the absence or the presence of the inducer IPTG. Each experiment included three biological replicates and three experiments were performed; representative data sets are shown.

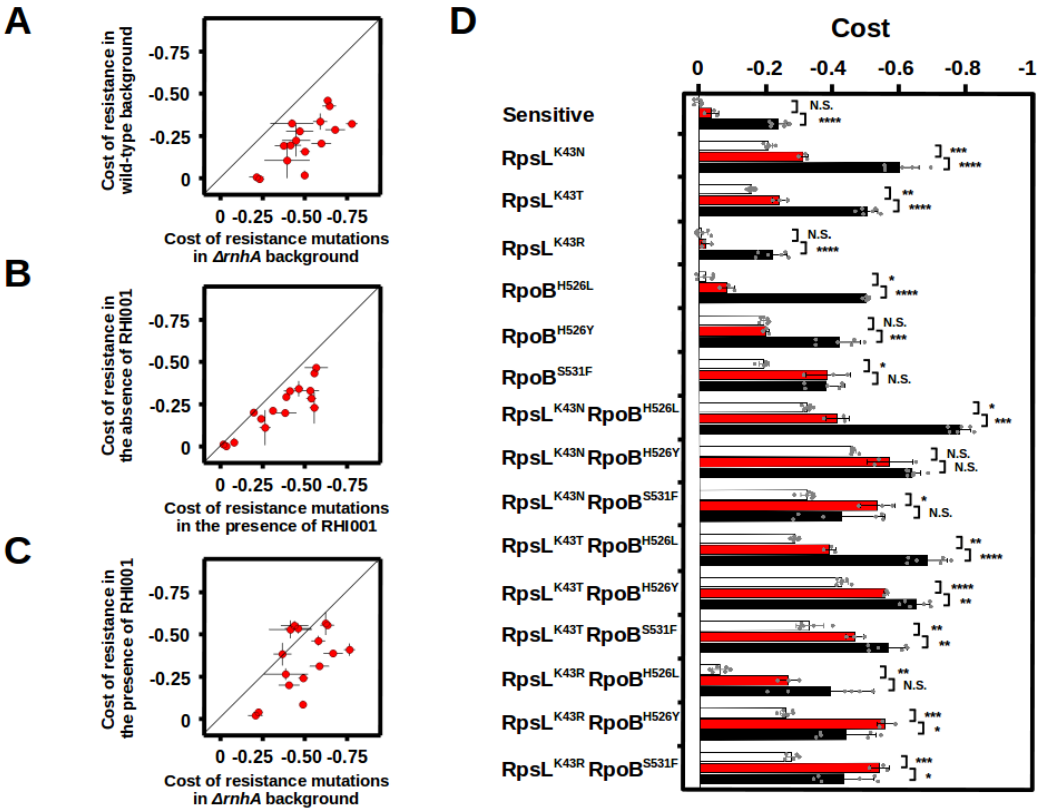

Figure 4. RNAse HI strongly influences the fitness of resistant bacteria. A. Correlation between the fitness cost of resistance mutations in wild-type (y axis) or *ΔrnhA* backgrounds (x axis). **B.** Correlation between the fitness cost of resistance mutations in the absence of the RNase HI inhibitor (y axis) or in its presence (x axis). **C.** Correlation between the fitness cost of resistance mutations in the presence of the RHI001 (y axis) or in the *ΔrnhA* background (x axis). The values corresponding to the wild-type background in panel A and to absence of RHI001 in panel B are those shown in Figure 1A. Error bars represent mean ± standard deviation of independent biological replicates (n≥3). The black line in panels A-C represents the linear regression if the costs were identical **D.** Fitness cost of sensitive bacteria and Str^R and/or Rif^R mutants in the presence of the RNase HI inhibitor RHI001 (red bars). For comparison, the corresponding values in the absence of the inhibitor (data from the experiments shown in Figure 1A) or in a *ΔrnhA* background (data from the experiments shown in panel A and Figure S4A) are represented as white and black bars, respectively. Error bars represent mean ± standard deviation of independent biological replicates (n=3). N.S. non-significant; $*P < 0.05$; $**P < 0.01$; $***P < 0.001$; $****P < 0.0001$ (two-tailed Student's *t* test). See also Figures S4, S5 and S6.

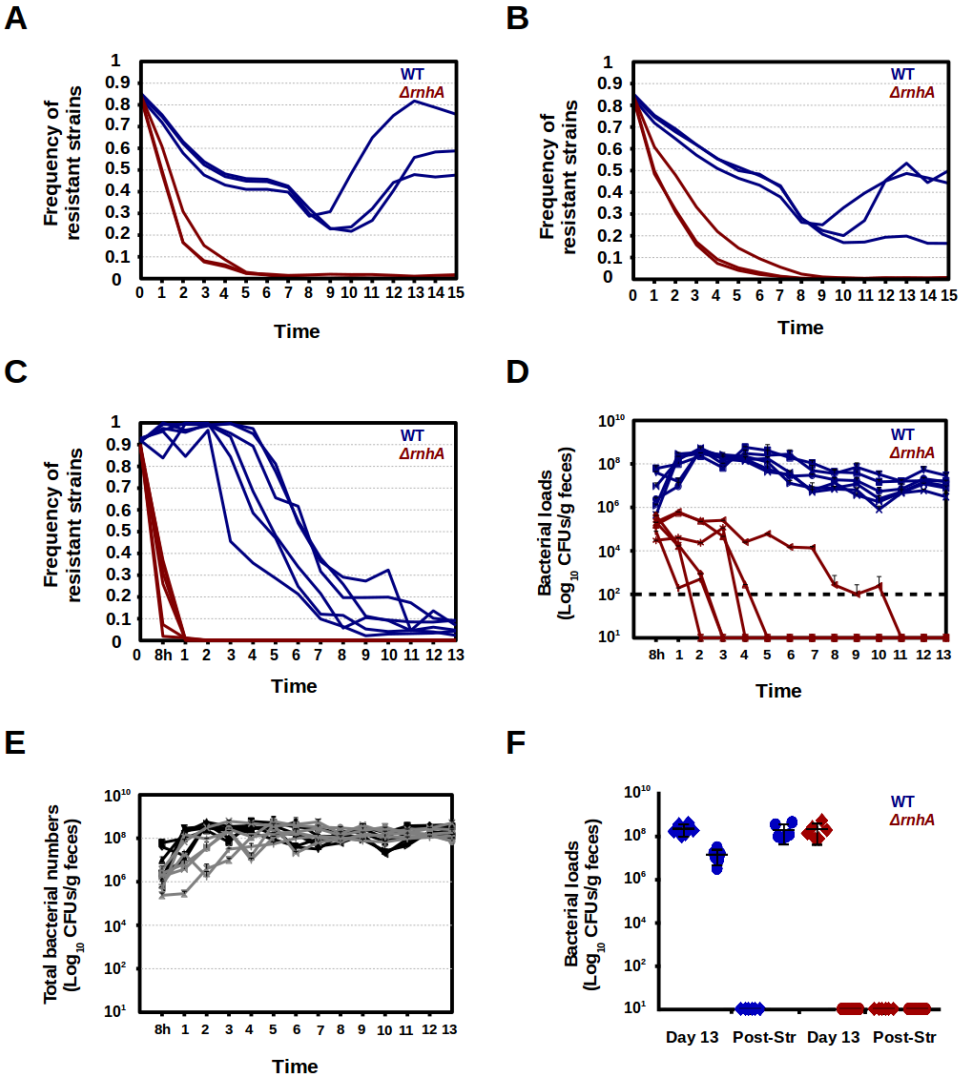

Figure 5. Lack of RNase HI favors outcompetition of resistant mutants by sensitive bacteria. A and B. Frequency of single resistant mutants during three independent long-term competitions in rich medium against sensitive bacteria either in a genetic background including RNase HI (blue lines) or in a *ΔrnhA* background (red lines), imposing a strong (1:1500 dilutions, **A**) or a mild (1:50 dilutions, **B**) bottlenecks. **C and D**. Frequency (**C**) and bacterial loads (Log_{10} CFUs/g og feces, **D**) of double resistant mutants during six independent long-term competitions against sensitive bacteria in mice, either in genetic backgrounds including RNase HI (blue lines) or in *ΔrnhA* backgrounds (red lines). Data are represented until extinction was observed in all six animals (13 days in the competitions in *ΔrnhA* backgrounds). The black dashed line represents the limit of detection. **E.** Total (sensitive + double mutant) bacterial loads (Log_{10} CFUs/g of feces) of the strains carrying RNase HI (black lines) or in the *ΔrnhA* background (grey lines) during the competitions in the mouse gut. **F.** Bacterial loads (Log_{10} CFUs/g og feces) at day 13 after gavage and after the week-long streptomycin treatment of sensitive (diamonds) and double resistant bacteria (circles) either in a genetic background carrying RNase HI (blue) or in a *ΔrnhA* background (red). Error bars represent mean ± standard deviation of the results in different mice (n=6).

Tables

Table 1. Percentage of cells showing DNA breaks (Gam-GFP foci) in sensitive and resistant bacteria either in wild-type or *ΔrnhA* backgrounds. Except in the *Δdam* positive control (in which over 100 cells sufficed to provide an illustrative example), at least 1000 cells per group were analyzed. See also Figures S1 and S2.

***Δdam* (positive control)**	**21.28%**
Sensitive	**0.72%**
rpsL (K43N)	**0.73%**
rpoB (H526Y)	**0.96%**
rpsL (K43N) rpoB (H526Y)	**10.71%**
***ΔrnhA* (sensitive)**	**9.27%**
ΔrnhA rpsL (K43N)	**33.92%**
ΔrnhA rpoB (H526Y)	**10.02%**
ΔrnhA rpsL (K43N) rpoB (H526Y)	**49.90%**

619 **Supplemental Figures**

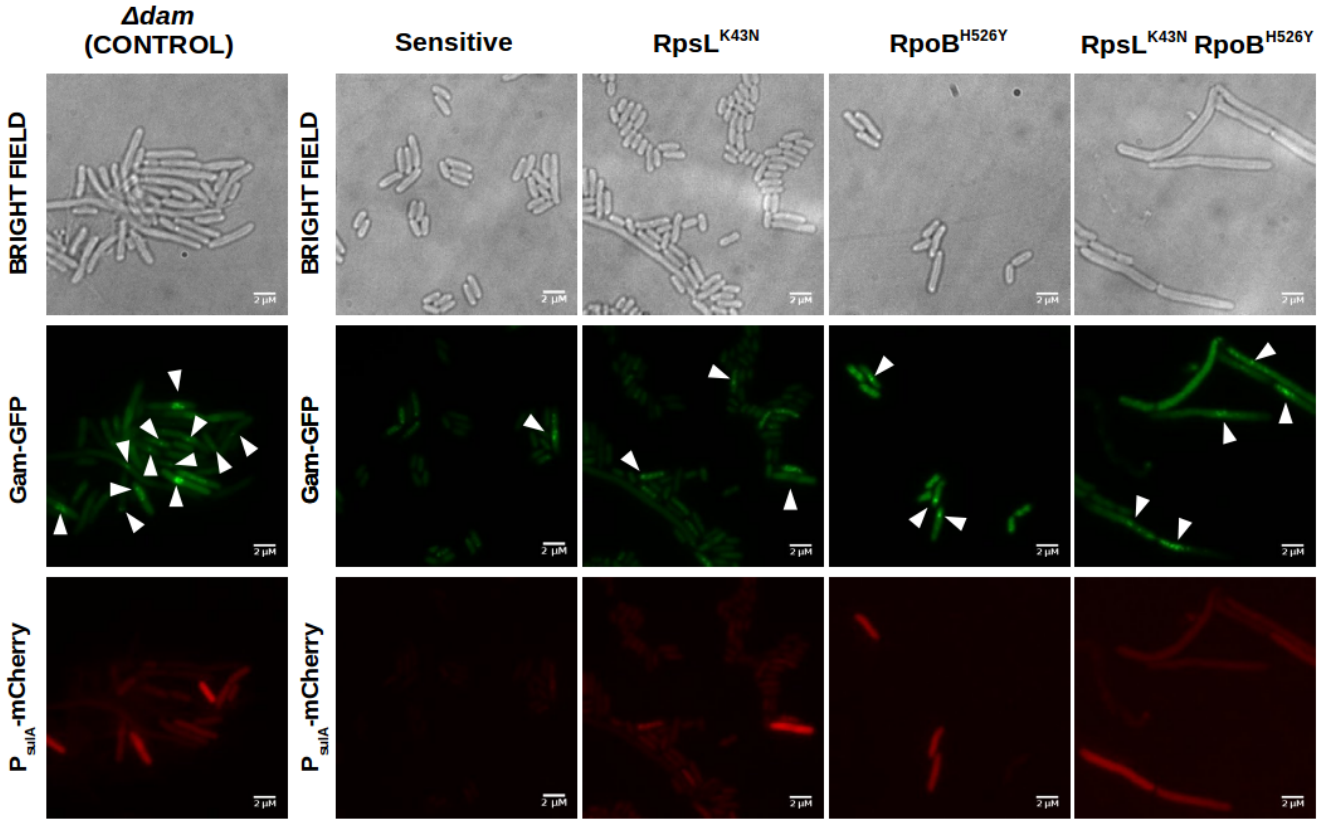

Figure S1. Visualization of DNA breaks and SOS induction of sensitive, single and double resistant strains by epifluorescence microscopy. Bacterial cells show a disperse faint green fluorescence distributed along the cytoplasm, unless DNA breaks are present; upon generation of DNA breaks, the disperse fluorescence concentrates in bright fluorescent foci (central panels, false-colored in green). Red fluorescence (bottom panels, false-colored in red) is absent until the SOS response is induced due to the presence of DNA breaks. Cell elongation (top panels) is a well-known phenotype derived from the inhibition of cell division by SOS-regulated proteins.

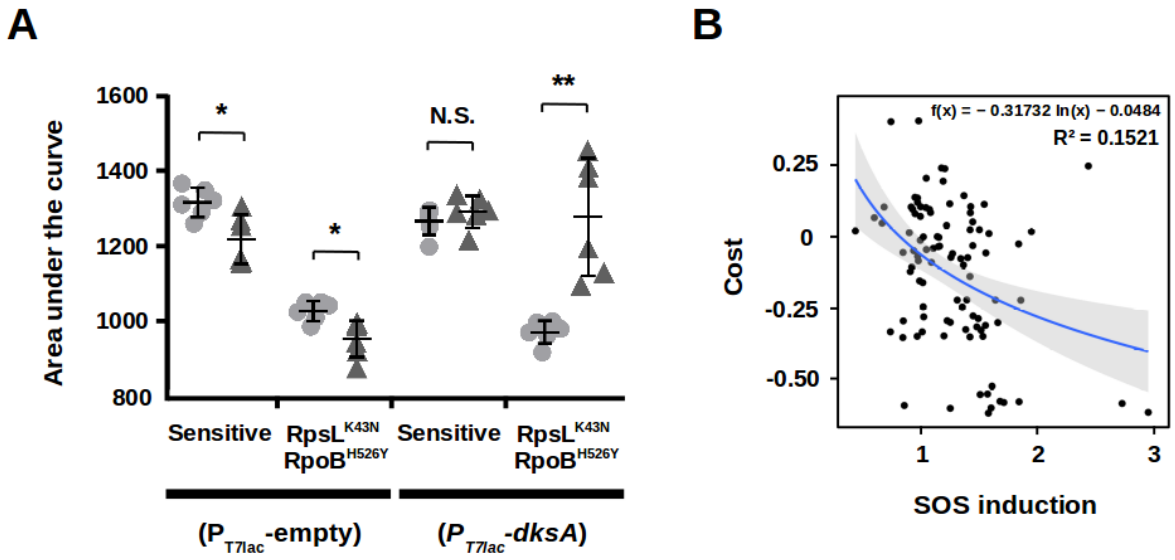

Figure S2. A. Area under the curve (24h in LB broth) of sensitive and double resistant bacteria harboring an expression vector either empty (left) or carrying the *dksA* gene in the absence (circles) or presence (triangles) of the inducer. Error bars represent mean ± standard deviation of independent biological replicates (n=6). N.S. non-significant; **P* < 0.05; ***P* < 0.01; ****P* < 0.001; *****P* < 0.0001 (two-tailed Student's *t* test). **B**. Correlation between the fitness cost (y axis) and the SOS induction (x axis) at 8h in M9 broth supplemented with 0.4% glucose (data represented in figure 3C). The blue line represents the logarithmic regression line, and the grey area represents the 95% confidence interval.

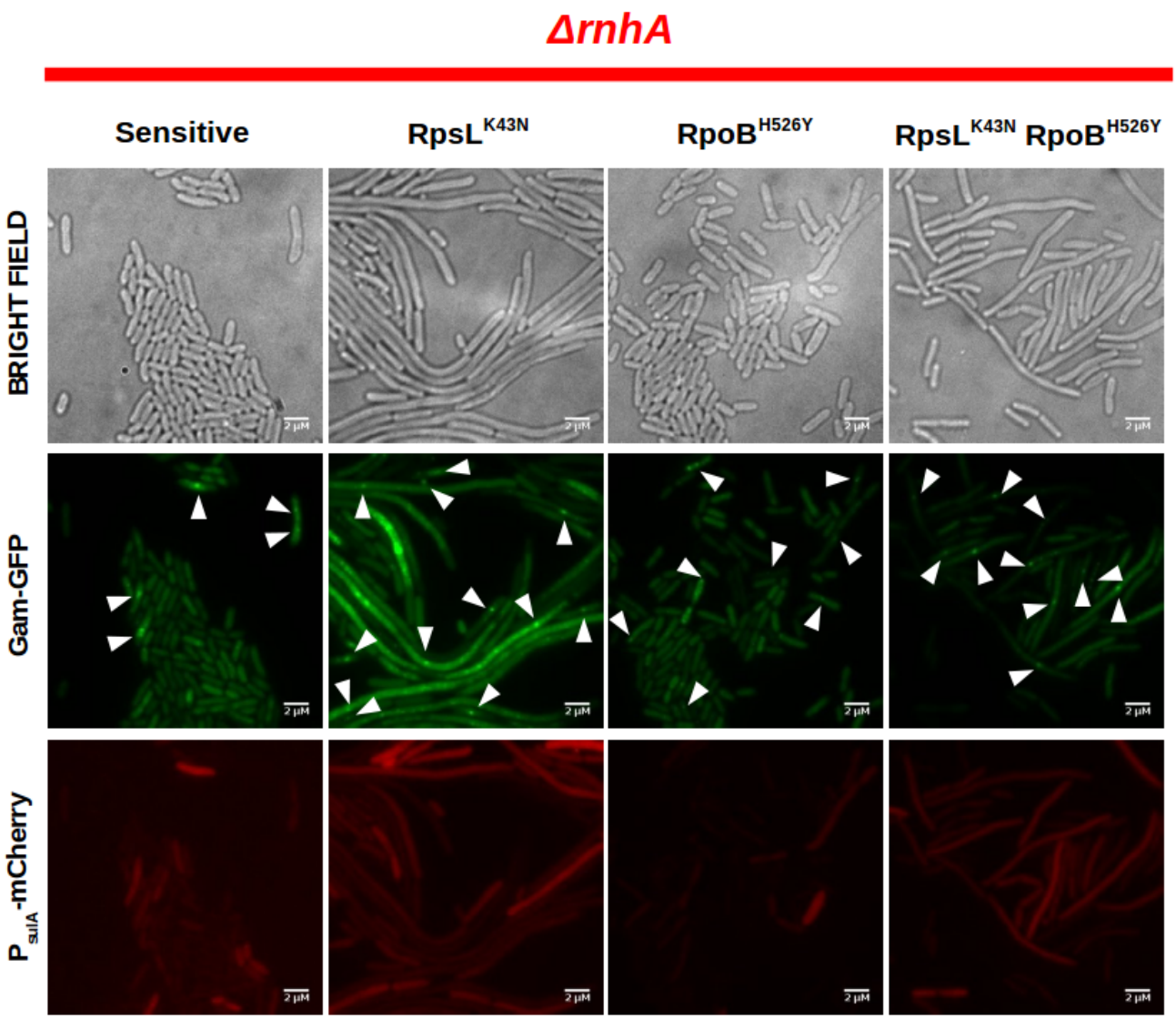

634 **Figure S3. Visualization of DNA breaks and SOS induction of sensitive, single and double resistant strains**
635 **in *ΔrnhA* background by epifluorescence microscopy.** Bacterial cells show a disperse faint green fluorescence
636 distributed along the cytoplasm, unless DNA breaks are present; upon generation of DNA breaks, the disperse
637 fluorescence concentrates in bright fluorescent foci (central panels, false-colored in green). Red fluorescence
638 (bottom panels, false-colored in red) is absent until the SOS response is induced due to the presence of DNA
639 breaks. Cell elongation (top panels) is a well known phenotype derived from the inhibition of cell division by
640 SOS-regulated proteins.

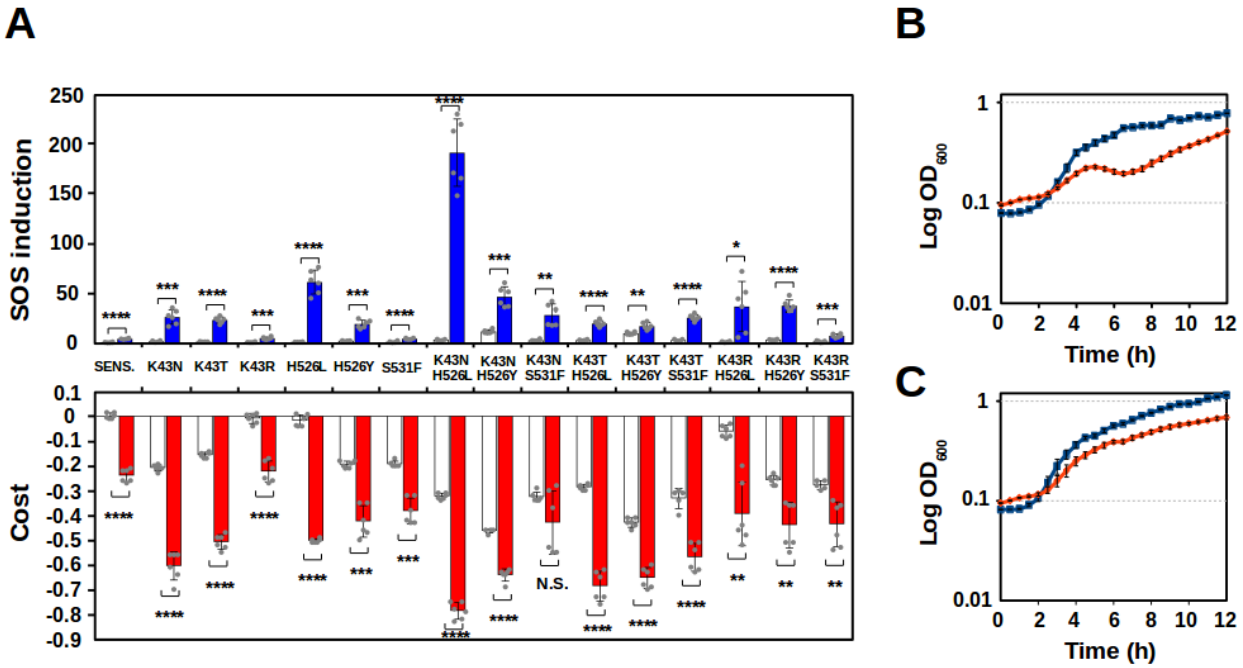

Figure S4. Depletion of RNase HI increases fitness cost and SOS induction. A. SOS induction (blue bars) and fitness cost (red bars), of sensitive bacteria and Str^R and/or Rif^R mutants (labels represent the corresponding allele/s) in a *ΔrnhA* background. White bars represent the corresponding values in bacteria with an intact *rnhA* gene (data from the experiments shown in Figure 1A), for comparison. Error bars represent mean ± standard deviation of independent biological replicates (n=6). N.S. non-significant; $*P < 0.05$; $**P < 0.01$; $***P < 0.001$; $****P < 0.0001$ (two-tailed Student's *t* test). **B.** Growth curves of $RpsL^{K43N}$ $RpoB^{H526Y}$ double mutant in the presence of either DMSO (blue lines) or RHI001 (orange lines). Points and error bars represent mean ± standard deviation of independent biological replicates (n=3). **C.** Growth curves of sensitive bacteria in the presence of either DMSO (blue lines) or RHI001 (orange lines). Points and error bars represent mean ± standard deviation of independent biological replicates (n=3).

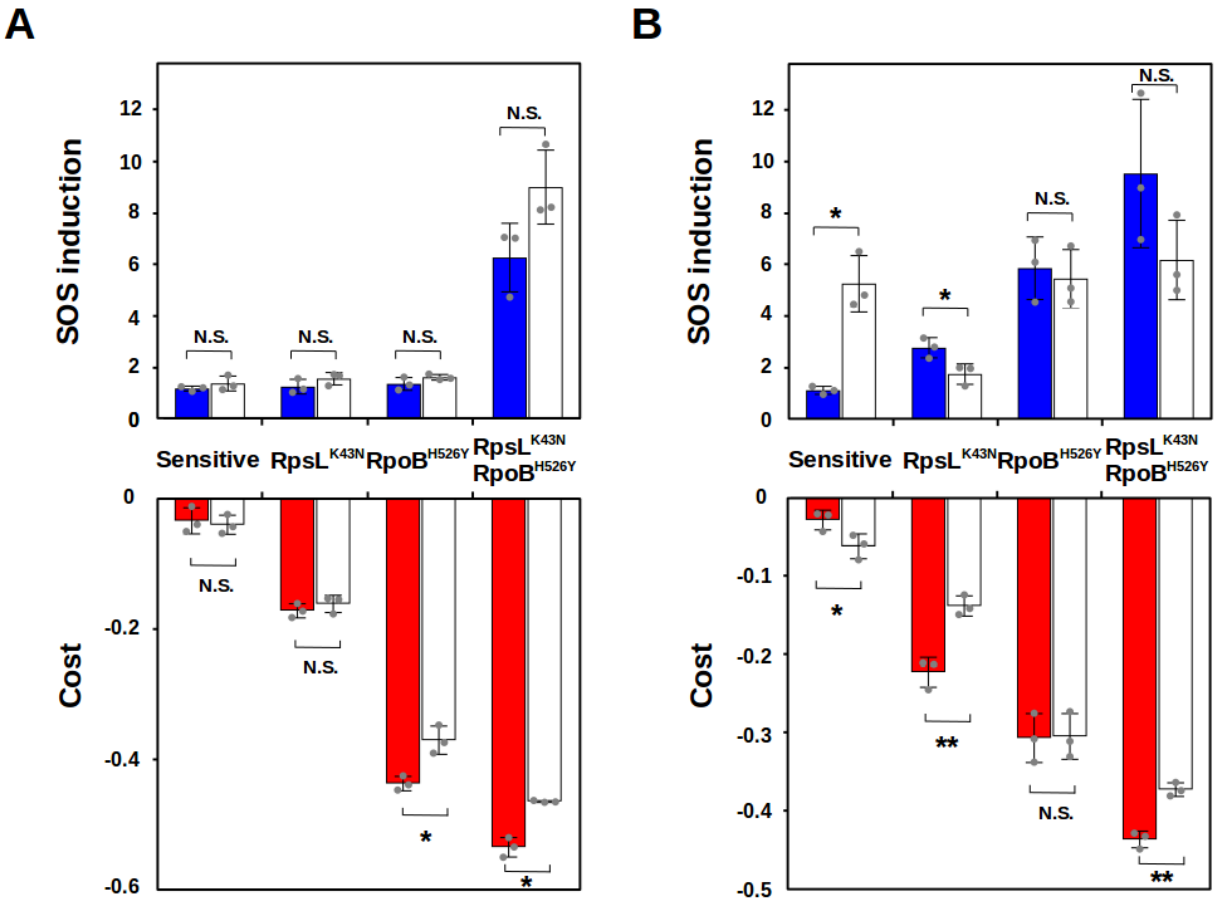

Figure S5. Mild overproduction of RNase HI can ameliorate both cost and SOS induction. SOS induction (top) and fitness cost (bottom), of sensitive bacteria (left), two single resistant mutants (center) and the double mutant combining these two alleles (right) in LB broth at 4h (**A**) or 24h (**B**) in a background harboring an additional chromosomal copy of the gene encoding the RNase HI (*rnhA*) under the control of the arabinose promoter, either in the absence (red bars) or the presence (white bars) of arabinose. Error bars represent mean ± standard deviation of independent biological replicates (n=3). N.S. non-significant; *$P < 0.05$; **$P < 0.01$; ***$P < 0.001$; ****$P < 0.0001$ (two-tailed Student's *t* test).

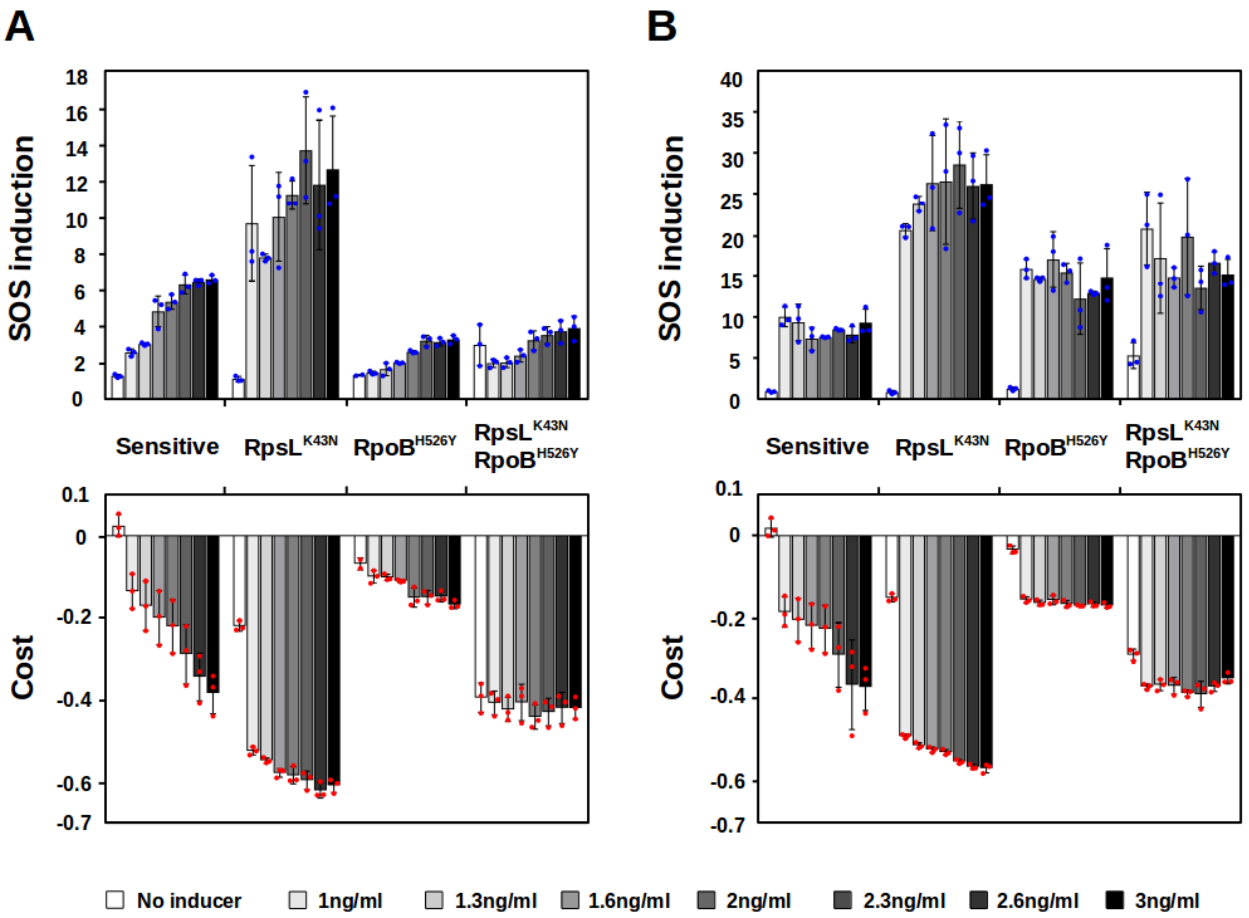

Figure S6. Strong overproduction of RNase HI increases cost and SOS induction in all the backgrounds. SOS induction (top) and fitness cost (bottom), of sensitive bacteria (left), two single resistant mutants (center) and the double mutant combining these two alleles (right) in LB broth at 4h (**A**) or 24h (**B**) in a background harboring a plasmid carrying a copy of the RNase HI gene (*rnhA*) under the control of a promoter inducible by anhydrotetracycline, either in the absence (white bars) or the presence of different concentrations of the inducer (greyscale, from light grey to black bars). Error bars represent mean ± standard deviation of independent biological replicates (n≥2). N.S. non-significant; **P* < 0.05; ***P* < 0.01; ****P* < 0.001; *****P* < 0.0001 (two-tailed Student's *t* test).
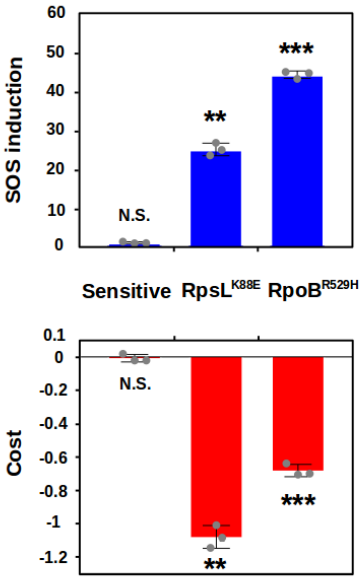
Figure S7. Costly single mutants show increased SOS induction. SOS induction (blue bars) and fitness cost (red bars), of sensitive bacteria (left) and two costly single resistant mutants (center and right). Error bars represent mean ± standard deviation of independent biological replicates (n=3). N.S. non-significant; *P < 0.05; **P < 0.01; ***P < 0.001; ****P < 0.0001 (two-tailed Student's t test).